



Published in final edited form as:

Nat Neurosci. 2016 November ; 19(11): 1477–1488. doi:10.1038/nn.4400.

Chd8 mediates cortical neurogenesis via transcriptional regulation of cell cycle and Wnt signaling

Omer Durak^{1,2}, Fan Gao¹, Yea Jin Kaeser-Woo¹, Richard Rueda¹, Anthony J. Martorell^{1,2}, Alexi Nott¹, Carol Y. Liu¹, L. Ashley Watson¹, and Li-Huei Tsai^{1,2,3,4}

¹Picower Institute for Learning and Memory, Massachusetts Institute of Technology, 77 Massachusetts Avenue, Building 46, Room 4235A, Cambridge, MA 02139, USA

²Department of Brain and Cognitive Sciences, Massachusetts Institute of Technology, 77 Massachusetts Avenue, Building 46, Room 4235A, Cambridge, MA 02139, USA

³Broad Institute of Harvard and MIT, Cambridge, MA 02139, USA

Abstract

De novo mutations in *CHD8* are strongly associated with autism spectrum disorder (ASD), however the basic biology of CHD8 remains poorly understood. Here we report that *Chd8* knockdown during cortical development results in defective neural progenitor proliferation and differentiation that ultimately manifests in abnormal neuronal morphology and behaviors in adult mice. Transcriptome analysis revealed that while *Chd8* stimulates the transcription of cell cycle genes, it also precludes the induction of neural specific genes by regulating the expression of PRC2 complex components. Furthermore, knockdown of *Chd8* disrupts the expression of key transducers of Wnt signaling, and enhancing Wnt signaling rescues the transcriptional and behavioral deficits caused by *Chd8* knockdown. We propose that these roles of *Chd8* and the dynamics of *Chd8* expression during development help negotiate the fine balance between neural progenitor proliferation and differentiation. Together, these observations provide new insights into the neurodevelopmental role of *Chd8*.

Users may view, print, copy, and download text and data-mine the content in such documents, for the purposes of academic research, subject always to the full Conditions of use: http://www.nature.com/authors/editorial_policies/license.html#terms

⁴Correspondence: Li-Huei Tsai, lhtsai@mit.edu, (O): 617-324-1660, (F): 617-324-1657.

Accession Codes

Sequencing data are available from the NCBI Gene Expression Omnibus (GEO) database under accession number GSE72442.

Data Availability

Sequencing data are available from the NCBI Gene Expression Omnibus (GEO) database under accession number GSE72442. Additional data that support the findings of this study are available upon request.

Author Contributions

O.D. and L.-H.T. designed the study, and L.-H.T. directed and coordinated the study. O.D. initiated, planned and performed the experiments. F.G. conducted the bioinformatics analysis. Y.J.K. cloned the human CHD8 construct and contributed to sample preparation for FAC-sorting. R.R. prepared cultured various cell lines and helped with sample preparation for FAC-sorting. A.J.M. conducted some of the luciferase assays. A.J.M. and A.N. contributed to behavioral experiments. C.Y.L. conducted the neuronal morphology experiments. L.A.W. conducted the *in situ* hybridization assay. O.D. and L.-H.T. wrote the manuscript with critical input from all of the authors.

Conflict of Interest

The authors declare no conflict of interest.

Introduction

Autism spectrum disorder (ASD) is a complex developmental disorder that manifests in social deficits, communication difficulties, stereotyped behaviors, and cognitive delays^{1,2}. Around 120 genes have been linked to ASD, often encoding proteins involved in chromatin remodeling, transcriptional regulation, and synapse function³⁻⁸. Of these, at least 15 distinct mutations in the coding regions of chromodomain helicase DNA binding protein 8 (*CHD8*), an ATP-dependent chromatin remodeler, were identified in ASD subjects from exome sequencing of trio families^{5,8,9}. Most of these mutations are predicted to be loss-of-function⁹. Subjects with *CHD8* mutations often display increased head circumference, cognitive deficits, as well as social interaction and communication difficulties^{5,9}.

Little is known about the biological function of CHD8. It was initially identified as a binding partner and negative regulator of β -catenin signaling and was shown to be enriched in the promoters of transcriptionally active genes¹⁰⁻¹³. Homozygous deletion of *Chd8* in mice results in early embryonic lethality resulting from massive apoptosis^{13,14}. However, there was no induction of Wnt/ β -catenin signaling in *Chd8* null mice¹⁴. CHD8 was also shown to be necessary for E2F1-dependent cell cycle gene activation during the G1/S transition¹¹. Down-regulation of CHD8 in cultured cells resulted in impaired cell proliferation¹⁵. In contrast, an increase in the number of mitotic cells and head size were observed following suppression of the *chd8* ortholog in zebrafish¹⁶.

Whereas the genetic and molecular underpinnings of ASD are heterogeneous, an accumulating body of evidence indicates that disrupted embryonic cortical development could be one of numerous defects underlying the etiology of ASD^{2,17,18}. Cortical development is a spatially and temporally regulated process that is defined by an early expansion of proliferative neural progenitor cells (NPCs) that reside in the ventricular zone (VZ) of cortical epithelium^{19,20}. At the onset of neurogenesis, NPCs undergo neurogenic divisions to produce pyramidal neurons that migrate radially to the cortical surface to generate the six layers of the neocortex²¹. Diverse signaling pathways govern the intricate balance between continued proliferation and cell cycle exit/differentiation. Of these, the role of canonical-Wnt signaling in cortical neural progenitor proliferation has been described extensively²²⁻²⁵. For instance, induction of Wnt signaling via overexpression of stabilized β -catenin increases neural progenitor proliferation by negatively regulating cell cycle exit/differentiation²⁶. In addition to signaling mechanisms, epigenetic mechanisms also play a crucial role in the spatial and temporal control of developmental genes^{21,27}. For instance, polycomb group (PcG) proteins are important for maintaining genes necessary for differentiation in a temporally repressed, but poised state, which allows for their activation in response to the appropriate differentiation cues^{27,28}.

Here, we examine the *in vivo* effects of Chd8 disruption on embryonic mammalian brain development. We show that *in utero* knockdown of Chd8 results in reduced cortical neural progenitor proliferation and altered neurogenesis. Transcriptional profiling of cortical neural progenitors via RNA sequencing (RNA-seq) following Chd8 knockdown showed that down-regulated genes were enriched for cell cycle control and chromatin remodeling pathways. Up-regulated genes were highly enriched for repressive H3K27me3 chromatin, potentially

due to reduced PRC2 complex activity. In contrast to previous *in vitro* findings in non-neuronal proliferating cells, our results indicate that Chd8 is a positive regulator of Wnt signaling in cells of neural lineage both *in vivo* and *in vitro*. Finally, knockdown of Chd8 in developing cerebral cortex resulted in behavioral deficits in adult mice, which can be rescued upon overexpression of β -catenin. Together, these observations provide new insights into the roles of Chd8 in brain development, and how mutations in *CHD8* may contribute to ASD.

Results

Chd8 is Highly Expressed in the Developing Brain

To understand whether *CHD8* has a role in cerebral cortical development, we first examined the temporal expression pattern of Chd8 in the developing mouse cortex. Quantitative polymerase chain reaction (qPCR) analysis demonstrated that *Chd8* is highly expressed in the embryonic day 12 (E12) cortex, and that its expression decreases with the progression of corticogenesis (Supplementary Figure 1a). Furthermore, an assessment of *CHD8* expression in the developing human dorsolateral and medial prefrontal cortex (DFC, MFC)²⁹ revealed that *CHD8* is highly expressed in both DFC and MFC during early fetal development. *CHD8* expression peaks in early mid-fetal period in DFC and early fetal period in MFC. The temporal expression pattern of *CHD8* in the developing human DFC and MFC was very similar to that of mouse *Chd8*, with reduction in expression throughout early development (Supplementary Figure 1b,c). Finally, *in situ* hybridization experiment revealed that *Chd8* is ubiquitously expressed in the developing cortex, and that in agreement with the results from our qPCR data above, *Chd8* expression in E12 cortex was higher than in E16 cortex (Supplementary Figure 1a,d). These initial studies suggest that *Chd8* could play an important role in cortical neural progenitor proliferation and differentiation.

Chd8 is Required for Cortical Neural Progenitor Proliferation

To determine the functions of Chd8 in the developing mouse cortex and because the ASD-associated *CHD8* mutations are predicted to lead to the loss of protein function^{5,9}, we used two distinct shRNAs (sh1 and sh2) to knockdown *Chd8*. Transfection of N2a cells with these shRNAs led to robust reduction of endogenous *Chd8* expression, as well as reduced expression of *Ccne2*, a previously identified target of Chd8 (Supplementary Figure 2a,b). Next we performed *in utero* electroporation to knockdown *Chd8* in cortical progenitors at E13, and analyzed brains at E16. Either scrambled shRNA (Control) or Chd8 shRNAs expression constructs were used, in combination with a GFP expression construct to label electroporated cells. We first examined the distribution of GFP-positive (GFP⁺) cells in the embryonic mouse cerebral wall. A significant reduction in the number of GFP⁺ cells was observed in the ventricular zone/subventricular zone (VZ/SVZ) of *Chd8* knockdown animals compared to controls, along with a comparable increase in the number of GFP⁺ cell in the cortical plate (CP; Figure 1a,b). To examine if the loss of GFP⁺ cells from the VZ/SVZ was due to reduced neural progenitor proliferation, we pulse-labeled with BrdU 24 hours prior to analysis. The brains were immunolabeled with antibodies against BrdU, the proliferative marker Ki67, and GFP. *Chd8* shRNAs caused a significant decrease in BrdU incorporation in the GFP⁺ cell population (Figure 1a,c). The reduction in cell proliferation was

accompanied by increased cell cycle exit (Figure 1a,d). We further used phosphorylated histone-H3-S10 (pHH3) to label mitotically active cells and observed a significant decrease in mitotic activity in *Chd8* knockdown embryos (Figure 1e,f). This was accompanied by a concomitant increase in the percentage of cells positive for neuronal marker Tuj1 (Figure 1e,g). In addition to this, we observed that *Chd8* knockdown caused a reduction in Sox2⁺ neural progenitors (Supplementary Figure 3a,b), but that apoptosis was unaffected (Supplementary Figure 3a,c). These results, together with the increased number of GFP⁺ cells in the cortical plate and the reduced number of BrdU⁺ cells, indicated that *Chd8* knockdown resulted in a premature depletion of the neural progenitor pool in the developing mouse cortex.

We next electroporated an shRNA-resistant human *CHD8* (hCHD8) overexpression construct in conjunction with the control and *Chd8* shRNAs (Supplementary Figure 2c). First, we found that overexpression of hCHD8 together with the control shRNA caused increased BrdU incorporation and mitotic activity, as well as reduced cell cycle exit and neuronal differentiation (Figure 1). Co-expression of hCHD8 with mouse *Chd8* shRNAs was able to restore levels of BrdU incorporation, mitotic activity and cell cycle exit, as well as normalize the distribution of GFP⁺ cells and the percentage of Tuj1⁺ cells to control levels (Figure 1). These experiments indicated that neural progenitor pool depletion and increased Tuj1⁺ neurons in the embryonic brain following that *Chd8* knockdown could result in a reduction in the total number of neurons produced in postnatal brain.

Chd8 is Important for the Expression of Cell Cycle Genes

To gain a deeper insight into how Chd8 regulates neural progenitor proliferation, we examined the transcriptome of neural progenitors following *Chd8* knockdown. We performed *in utero* electroporation, targeting NPCs at E13, and using either control or *Chd8* shRNAs together with a GFP expression construct. The GFP⁺ cell population was then isolated through fluorescence-activated cell sorting (FAC-sorting) 48 hours following the *in utero* transfection. This approach ensured that our analysis included only transfected cell populations with the same birthdate. Following total RNA collection, we performed next-generation sequencing to identify differentially expressed genes (DEGs) between control and *Chd8* knockdown cells (Figure 2a and Supplementary Dataset S1).

Our analysis revealed a total of 3762 genes in the *Chd8* sh1 and 5245 genes in the *Chd8* sh2 knockdown samples that were differentially expressed compared with control samples (p-value < 0.05 & Fold Change > 1.2; Dataset S2 and S3; Supplementary Figure 4). To identify biological functions perturbed by *Chd8* knockdown, we subjected the DEGs to gene ontology analysis of biological processes which showed that genes down-regulated by *Chd8* knockdown are involved in regulation of cell cycle, chromosome organization, RNA processing, and cytoskeleton organization (Figure 2b, Supplementary Dataset S4 and S5). Up-regulated genes in *Chd8* knockdown samples were enriched for processes relating to neuronal development such as neuron/cell differentiation, cell migration, and defense response (Figure 2b, Supplementary Dataset S6 and S7). Supporting the analysis of biological processes, an analysis of the biological pathways enriched in the down-regulated genes revealed pathways relating to cell cycle, DNA replication and Wnt signaling

(Supplementary Figure 5, and Supplementary Dataset S8 and S9). Furthermore, mammalian (mouse) phenotype analysis of down-regulated genes were enriched for categories such as prenatal lethality, abnormal embryo/brain size, and abnormal brain development. Together these analyses suggest that *Chd8* has an essential role in regulating prenatal genes necessary for proper embryonic development. We then validated a subset of downregulated (*Akap8*, *Cdc7*, *Tacc3*, *Timeless*, *Notch2*, *Kif20b*, *Dnmt3a* and *Tial1*) and upregulated (*Camk1d*, *Pak6*, *Fgf8* and *Jakmip1*) genes via qPCR, and correlated these changes in expression with RNAseq data which showed significant Pearson and Spearman correlation coefficient (Figure 2c).

Our results are consistent with previous studies that have assessed the transcriptional consequences of *Chd8* suppression^{12,16,30,31}. For instance, Sugathan *et al.* showed that, in hNPCs, CHD8 regulates genes highly expressed in developing brain and important for neurodevelopmental pathways¹⁶. Similarly, other studies have shown that genes dysregulated following *CHD8* knockdown transcriptionally regulate cell cycle progression and neuronal differentiation^{12,30,31}. Furthermore, gene ontology of biological functions for chromatin organization and regulation of transcription were enriched in all dysregulated gene datasets. Overall, these results suggest that *Chd8* has a dual role in regulating gene expression: 1) it promotes the expression of genes necessary for prenatal development and important for cell cycle progression, and 2) represses the expression of genes important for neuronal differentiation and maturation in embryonic cortical NPCs.

In addition to these results, we compared DEGs following *Chd8* knockdown to SFARI AutDB gene database³², and found that a substantial proportion of DEGs following *Chd8* knockdown (sh1; 183 and sh2; 215) were SFARI ASD risk genes (Supplementary Figure 6a,b and Supplementary Dataset S10). These findings in the developing mouse brain suggest that *Chd8* is an apical factor in the regulation of ASD risk genes.

Chd8 Is a Transcriptional Activator of Genes Necessary for Early Cortical Development

To gain further insight into the molecular mechanisms by which *Chd8* controls gene expression during embryonic brain development, we generated a chromatin states map for the E12 mouse brain based on published chromatin immunoprecipitation-sequencing (ChIP-seq) data for seven chromatin marks (ENCODE, www.encodeprojects.org). Genomic regions were classified into different chromatin states defined by combinations of these histone marks, including promoters, enhancers, transcribed, bivalent, repressed and low signal regions (Supplementary Figure 7)³³. We then mapped CHD8 peaks from hNPCs¹⁶, hNSCs¹² and human midfetal DFC¹² ChIP-seq datasets and *Chd8* peaks from E17.5 mouse cortex ChIP-seq dataset¹² to our chromatin states map (Figure 3a). Both human and mouse *Chd8* binding peaks were highly enriched for chromatin states associated with active promoters (Figure 3a), suggesting that *Chd8* binds to the promoters of actively transcribed genes. We then examined the overlap between CHD8 ChIP-seq peaks in hNSCs with differentially expressed genes in both of our *Chd8* knockdown datasets, and found that 58.4% (367/628) of the differentially expressed genes following *Chd8* knockdown contained CHD8 ChIP-seq peaks in their promoters (Figure 3b). A significant majority of these 367 differentially expressed genes (291; 79.5%) were down-regulated following *Chd8*

knockdown. These results suggest that Chd8 could function as a transcriptional activator in mouse cortical progenitors (Figure 3b). Consistent with this possibility, we found that genes down-regulated by *Chd8* knockdown are normally enriched for H3K27ac, a chromatin mark associated with active gene promoters (Figure 3c). Thus, our data indicate that Chd8 functions primarily as a transcriptional activator in neural progenitors. Cotney *et al.* previously published similar findings wherein active histone marks were enriched at transcription starting sites of CHD8 target genes¹².

In contrast to the scenario with down-regulated genes, we observe that up-regulated genes following *Chd8* knockdown are normally enriched for H3K27me3, a chromatin mark associated with repressed gene promoters (Figure 3d). The levels of H3K27me3 are regulated through the activities of the PRC2 complex. Interestingly, our RNA-seq data revealed that the expression of two main components of the PRC2 complex, *Ezh2* and *Suz12*, were significantly attenuated upon *Chd8* knockdown. The effects of *Chd8* knockdown on these genes were further verified by qPCR (Figure 3e). Additionally, infection of cultured mNPCs with *Chd8* shRNA also caused a significant reduction in Ezh2 protein levels, which is the functional enzymatic component of the PRC2 complex (Figure 3f). Furthermore, published CHD8 ChIP-seq data sets show that CHD8 binds to the promoters EZH2 and SUZ12^{12,16}. These results suggest that *Chd8* knockdown could up-regulate genes directly targeted by PRC2 complex. In fact, from analysis of publicly available CHD8¹², Ezh2³⁴ and Suz12³⁵ ChIP-seq datasets, we find that among the fraction of up-regulated genes that lack *CHD8* binding within their promoters, a significant proportion (approximately 25%) are normally bound by Ezh2/Suz12 (Figure 3g). These results suggest that the down-regulation PRC2 complex components could constitute an additional important mechanism by which Chd8 regulates gene expression.

Overall, our data provides key mechanistic insights into the dual function of Chd8 as a promoter of cell cycle progression, and a repressor of neural genes – Chd8 binds the promoters of cell cycle genes and serves as a transcriptional activator. At the same time, it also promotes PRC2 expression that allows for the repression of neural genes during this developmental period.

Chd8 maintains Wnt signaling in neural progenitors

While *Chd8* knockdown caused the down-regulation of a number of genes related to cell cycle progression, gene ontology of biological pathways analysis indicated that genes encoding for the Wnt signaling pathway were enriched among the genes down-regulated in *Chd8* knockdown samples (Supplementary Figure 5). These include several of the primary transducers and effectors of the Wnt signaling pathway, such as *Fzd1*, *Fzd2*, *Dvl2*, *Dvl3* and *Ctnnb1* (Supplementary Dataset S2 and S3). Transcriptional dysregulation of Wnt/ β -catenin signaling by CHD8 in NSCs has also been reported previously^{12,16,30,31}. To validate the findings from RNA-seq experiments, we processed FAC-sorted cells for qPCR analysis and found that Chd8 knockdown resulted in reduced expression of several Wnt signaling genes as well as a Wnt target gene (*Cnd1*, Figure 4a). To understand whether Chd8 directly targets these genes, we performed Chd8 ChIP-qPCR experiments using mouse embryonic cortical tissue (E12), and found that Chd8 binds to the promoter regions of *Fzd1*, *Dvl3* and

Cttnb1 genes (Supplementary Figure 8b). Consistent with these results, analysis of publicly available human and mouse Chd8 ChIP-seq datasets revealed the enrichment of Chd8 at the promoters of *FZD1/Fzd1*, *FZD2/Fzd2*, *DVL2/Dvl2*, *DVL3/Dvl3* and *CTNNB1/Cttnb1* (Supplementary Figure 8a)^{12,16}. Together, these findings suggest that Chd8 is required for maintaining Wnt signaling in embryonic mouse cortical neural progenitors.

To further test this hypothesis, we used a luciferase reporter assay to measure Wnt-mediated transcriptional activity. First, we *in utero* transfected mouse embryonic NPCs with the luciferase construct along with either control or *Chd8* shRNA. Cerebral cortical tissues were harvested to measure luciferase reporter activity 72 hours later. We found that, following knockdown of *Chd8*, TCF/LEF-reporter activity was markedly reduced compared to controls (Figure 4b). In contrast, overexpression of h*CHD8* resulted in a significant increase in TCF/LEF-reporter activity (Figure 4b). Furthermore, co-expression of *Chd8* shRNA along with h*CHD8* cDNA restored the Wnt signaling activity (Figure 4b). Similarly, in N2a cells, both *Chd8* shRNAs markedly reduced Wnt signaling activity, and this effect can be normalized by co-expressing h*CHD8* cDNA alongside *Chd8* shRNAs (Figure 4c).

Contrary to our findings, previously published reports identified Chd8 as a negative regulator of canonical-Wnt/ β -catenin signaling^{10,13,36}. It is worth noting that these earlier studies were conducted in non-neuronal cells, suggesting that Chd8 could play cell-type specific roles in regulating Wnt signaling. We therefore examined Wnt signaling in a non-neuronal cell line to determine if the regulation of Wnt signaling by Chd8 is cell type-specific. We conducted the TCF/LEF luciferase assay using human embryonic kidney 293T (HEK293T) cells as used in Nishiyama *et al* (2011)³⁷. We observed a significant up-regulation in Wnt signaling activity following *CHD8* knockdown (Figure 4d), consistent with previous reports using non-neuronal cells^{10,13,36,37}. Surprisingly, *CHD8* knockdown did not affect the expression of Wnt signaling genes in HEK293T cells (Supplementary Figure 9). Furthermore, we also examined the consequences of Chd8 loss-of-function on TCF/LEF luciferase activity in both mouse and human cultured NPCs. We found that knockdown of *Chd8* caused reduced Wnt signaling activity in both mouse and human NPCs (Figure 4e,f). These results strongly suggest that the influence of Chd8 on Wnt signaling is cell type-specific, and that Chd8 is a positive regulator of Wnt signaling in cells of neural progenitors.

Increased β -catenin expression can counteract Chd8-knockdown-associated phenotypes

Our findings suggest that Chd8 could stimulate Wnt signaling activity in proliferating neural cell lines, in part through transcriptional regulation of multiple Wnt pathway components. β -catenin is the critical downstream component of the Wnt signaling pathway²³. Upon activation of canonical-Wnt signaling, β -catenin is stabilized in the cytoplasm and subsequently enters the nucleus, where it binds to TCF/LEF family transcription factors to activate expression of Wnt target genes such as *Ccnd1*²³. To determine if Chd8 regulates cortical progenitor proliferation via Wnt signaling, we expressed a degradation-resistant β -catenin mutant construct (S37A) alongside *Chd8* sh2. Expression of stabilized β -catenin rescued TCF/LEF luciferase activity following *Chd8* knockdown in embryonic mouse brain (E13-E16, Figure 5a) and in N2a cells (Figure 5b).

We next evaluated if increased Wnt signaling activity could also rescue reduced progenitor proliferation downstream of *Chd8* knockdown. We performed *in utero* electroporation at E13 with control or *Chd8* shRNA and co-expressed either control empty vector or stabilized β -catenin constructs. The pregnant dams were injected with BrdU 48 hours later at E15, and the embryos were harvested at E16. As shown earlier, we observed a significant shift of GFP⁺ cell from the VZ/SVZ to the CP in *Chd8* knockdown samples (Figure 5c,d). The altered distribution of GFP⁺ cells was normalized upon stabilized β -catenin co-expression (Figure 5c,d). Furthermore, stabilized β -catenin also rescued the levels of cell proliferation (Figure 5c,e), cell cycle exit (Figure 5c,f), increased Tuj1⁺ cells (Figure 5g,i), and normalized mitotic index (Figure 5g,h) phenotypes that occurred in response to *Chd8* knockdown.

Finally, we assessed whether the induction Wnt signaling could also ameliorate the transcriptional dysregulation caused by *Chd8* knockdown. To this end, we performed *in utero* electroporation at E13 using control or *Chd8* shRNA expression constructs and co-expressed either control empty vector or stabilized β -catenin constructs, respectively. Following FAC sorting of GFP⁺ cells at E15, the samples were subjected to RNA-seq as described above. Consistent with the effects of stabilized β -catenin on neurogenesis and Wnt luciferase activity, the expression of many dysregulated genes was normalized upon β -catenin stabilization (Supplementary Figure 10a and Supplementary Dataset S11). This is consistent with the findings that LEF1 consensus motif (CTTTGT) is the most significantly enriched transcription factor binding motif among genes down-regulated in response to *Chd8* sh2 knockdown (Supplementary Dataset S5). Additionally, the expression of both *Ezh2* and *Suz12* was restored to control levels following the expression of stabilized β -catenin (Dataset S11 and Figure Supplementary Figure 10b).

Together, these data underscore the role of Chd8 in maintaining Wnt signaling in embryonic cortical progenitors and indicate that impaired Wnt signaling following Chd8 knockdown underlies abnormal cortical progenitor proliferation, neuronal differentiation defects and transcriptional dysregulation of genes important for proper cortical development.

Reduced Chd8 Expression in Upper Layer Cortical Neurons in the Developing Brain Results in Behavioral Abnormalities in Adult Mice

To evaluate the possible outcome of reduced Chd8 function during cortical development in adult animals, we performed bilateral *in utero* electroporation at E15, which targets neurons destined to populate cortical layers 2/3, with either control or *Chd8* sh2 along with membrane bound GFP or cytoplasmic-GFP. Bilateral targeting of upper layer cortical neurons was examined in these animals following behavioral testing (Supplementary Figure 11a,b). No significant difference in basic locomotor activity was observed between the groups (Supplementary Figure 11d–h). Similarly, contextual fear conditioning test revealed no differences in learning behavior between the two groups (Supplementary Figure 11i). We then examined the conflict between exploration and risk avoidance using the light/dark box test³⁸. The *Chd8* shRNA group exhibited significant reductions in entries to and amount of time spent in the light chamber compared to controls (Figure 6a,b), suggesting increased aversion following Chd8 loss-of-function. We further employed the elevated plus maze³⁹.

The *Chd8* shRNA mice entered and spent significantly less time in the open arms of the maze compared to controls (Figure 6c,d), further supporting the notion that reduced *Chd8* expression in late cortical progenitor cells resulted in altered anxiety-dependent exploratory drive in adult mice.

One of the most commonly observed behavioral deficits in ASD and other psychiatric patients is abnormal social interaction. We used the three-chamber social arena assay⁴⁰ to examine the sociability of control and *Chd8* knockdown mice. In this assay mice are allowed to explore the empty arena during an initial habituation period, which is followed by a period where a novel mouse (Stranger) is held inside a wired cage in one of the lateral chambers and an identical cage with a novel inanimate object (Empty) is placed in the opposing lateral chamber. During the habituation period, both control and *Chd8* shRNA mice explored the two lateral chambers equally (Supplementary Figure 12a). When the novel mouse was introduced, as expected the control mice displayed a preference for the lateral chamber with the novel mouse, whereas the *Chd8* shRNA group did not show a preference for either chamber (Figure 6e). Furthermore, whereas control mice spent significantly more time in close interaction with the cage containing the novel mouse (within 5 cm), *Chd8* knockdown mice did not show any preference for either cage (Figure 6f). We did not observe any deficits in exploratory behavior as both groups spent similar amount of total time interacting with both the wired cages, suggesting that social interaction deficits in *Chd8* shRNA group cannot be attributed to lack of exploratory behavior (Supplementary Figure 12b). These data suggest that knockdown of *Chd8* in neural progenitors destined for upper layer cortical neurons manifests in reduced anxiety-dependent exploratory drive and abnormal social interaction behavior in adult mice.

Given that β -catenin overexpression could rescue the defects in Wnt signaling activity and cortical progenitor proliferation downstream of *Chd8* loss-of-function (Figure 5), we asked whether increased Wnt/ β -catenin signaling could also rescue the behavioral abnormalities associated with *Chd8* knockdown. To test this hypothesis, we performed *in utero* electroporation at E15 and expressed stabilized β -catenin alongside *Chd8* shRNA (Supplementary Figure F11c). Co-expression of stabilized β -catenin rescued the number of entries to light chamber (Figure 6a), amount of time spent in light chamber (Figure 6b), number of entries to open arms (Figure 6c) and time spent in open arms (Figure 6d). Furthermore, rescue group spent significantly more time in the chamber with novel social mouse (Figure 6e), and spent more time in close interaction (Figure 6f). These results suggest that impaired Wnt/ β -catenin signaling could underlie the behavioral deficits associated with *Chd8* loss-of-function.

To determine whether knockdown of *Chd8* expression in the developing cortex affects long-term neuronal abnormalities in the adult brain, we examined the number, localization, dendritic complexity and spine density of neurons. For these studies, the *in utero* electroporation was performed using shRNA constructs co-electroporated with either membrane bound-GFP or cytoplasmic-GFP. We observed a significant reduction in the number of GFP⁺ cells in *Chd8* knockdown brains (Supplementary Figure 13a,b). Furthermore, *Chd8* knockdown also resulted in mislocalization of GFP⁺ neurons in the adult brain (Supplementary Figure 13a,c). An assessment of dendritic arborization of layer 2/3

neurons using Sholl analysis revealed markedly reduced dendritic branching in *Chd8* knockdown samples compared to control neurons (Figure 6g,h). Additionally, measurement of total spine density on the secondary branches of apical dendrites showed significant reduction following *Chd8* knockdown (Supplementary Figure 13d,e). Finally, increased Wnt/ β -catenin signaling was sufficient to restore the complexity of dendritic arborization (Figure 6g,h). Reduced dendritic spine density in *Chd8* knockdown neurons were significantly increased following induction of Wnt/ β -catenin signaling, however, it did not reach the control levels (Supplementary Figure 13d,e). These results are consistent with previous findings showing that induced Wnt/ β -catenin signaling increases dendritic complexity and spine density^{41,42}. In sum, our observations suggest that *Chd8* plays a crucial role in establishing proper cortical circuitry, and that the disruption of neuronal morphology and neuronal connectivity due to *Chd8* loss-of-function could contribute to the observed behavioral abnormalities in adult mice.

Discussion

***Chd8* is essential for cortical progenitor proliferation and differentiation**

Our results indicate that the chromatin remodeler, *Chd8*, plays a crucial role in mammalian cortical development by promoting the proliferation of neural progenitors in two distinct ways. On the one hand, *Chd8* directly binds to the promoters of cell cycle genes, and facilitates their expression, while on the other *Chd8* also regulates neurogenic divisions by targeting the PRC2 complex. Previous studies have shown that the absence of *Ezh2* drives neural progenitors in the developing cortex towards neurogenic division²⁸. Together, these activities ensure the generation of appropriate numbers of neurons during cortical development.

An overwhelming body of literature on the role of CHD8 and other CHD proteins supports our findings. Depletion of *Chd8* resulted in reduced cell proliferation in mammalian cell lines^{11,15,43,44}. *Chd8* is closely related to *Chd6/7/9*. *Chd7*, an interacting partner of *Chd8*, has been shown to be necessary for proliferation of inner ear neuroblasts⁴⁵ and NSCs in the olfactory epithelium⁴⁶ in mice, as well as cellular proliferation in multiple tissues of zebrafish⁴⁷. Deletion of *ChdC* in *Dictyostelium*, an ortholog of the mammalian Class III CHD group which contains *Chd5–9*, impaired cell growth due to reduced expression of cell cycle genes⁴⁸. Interestingly, knockdown of *CHD8* in zebrafish caused an increase in the number of newborn neurons and resulted in macrocephaly, although there was a reduction in the number of enteric neurons in the GI tract^{9,16}. The reason for these differences is presently unclear. A more detailed and direct analysis of neural progenitor proliferation in zebrafish should clarify this matter. Our results suggest that embryonic *Chd8* knockdown would result in reduced number of neurons in the adult brain. However, because our experiments are limited to analysis of NPCs, we cannot elucidate the role of *Chd8* in development of other cell types such as astrocytes. It is possible that dysregulation of *Chd8* in other cells could alter the size or number of these cells, contributing to macrocephaly phenotype observed among ASD patients with CHD8 mutations.

Chd8 positively regulates Wnt signaling in neural progenitor cells

Canonical-Wnt signaling plays important roles in brain development through the regulation of cell cycle progression and dendritic morphogenesis²³. Importantly, defects in Wnt signaling have been strongly implicated in the development of ASD. Mutations in several pathway components have been identified in ASD patients, and convergent pathway analyses indicate that many apparently unrelated ASD mutations also impinge on the Wnt signaling pathway⁴⁹. Earlier work on the function of Chd8 demonstrated that it negatively regulates Wnt signaling. Unexpectedly however, we found that multiple components of canonical-Wnt signaling were down-regulated upon loss of Chd8 in neural progenitors. Our efforts to resolve these differences have led to the discovery that Chd8 regulates Wnt signaling in a cell-type specific manner – whereas CHD8 loss-of-function increases Wnt signaling in non-neuronal cells, its loss attenuates Wnt signaling in neural progenitors. Cell type-specific regulation by Chd8 is not unprecedented. *Drosophila* ortholog of Chd8, Kismet, regulates *hedgehog* (*hh*) expression in the wing imaginal disc in a context when expression of the repressor, Ci-75, is low⁵⁰. However, Kismet is not necessary for the regulation of *hh* expression when Ci-75 expression is high, suggesting a context-dependent function⁵⁰. A similar context-dependent mechanism could account for differences in regulation of Wnt signaling by Chd8. Overall, our observations suggest that whereas Chd8 promotes cell proliferation in both neural and non-neuronal cells, it selectively promotes Wnt signaling in neural progenitors.

Sustained expression of Chd8 in the developing cortex is necessary for normal adult behavior

Abnormal social interaction, anxiety and intellectual disability are some of the behavioral deficits observed among ASD patients carrying *CHD8* mutations⁹. Our results indicate that restricted Chd8 loss-of-function in developing mouse brain also produces behavioral deficits such as abnormal social interaction. Interestingly, normal adult behavior and proper cortical development were restored upon overexpression of stabilized β -catenin, indicating that behavioral abnormalities likely stem from abnormal cortical development. We did not observe any deficits in learning and memory; however, *Chd8* knockdown was confined to specific layers of the developing cortex. It is possible that Chd8 loss-of-function in other regions of the developing brain may affect additional behaviors. Future studies on the effects of whole brain Chd8 loss-of-function on adult behavior would be of importance. Thus, it remains to be determined whether the mechanisms described here apply to germline loss-of-function mutations observed in ASD subjects.

In sum, our observations suggest that in the developing mouse brain Chd8 maintains neural progenitor proliferation through regulation of cell cycle genes. Furthermore, our results raise the possibility that some of the ASD associated behavioral abnormalities in patients carrying *CHD8* mutations may be caused by impaired development of cerebral cortical regions. Though Chd8 may be regulating neural progenitor proliferation through different ways, induction of Wnt/ β -catenin signaling is sufficient to mitigate cortical development and adult behavioral deficits caused by *Chd8* knockdown.

Methods

DNA constructs

Control non-targeting shRNA (Sigma, SHC002), sh1 and 2 targeting *Chd8* were obtained from Sigma (sh1, Clone ID: NM_201637.1–1439s1c1 and sh2, Clone ID: NM_201637.2–3342s21c1). The sequences can be found on Supplementary Table 1. Full length hCHD8 was cloned into mammalian expressing pCMV5 vector. Super8XTOPFLASH, a gift from Dr. R. Moon (University of Washington, WA) and a Renilla-Luc-TK reporter (pRL-TK, Promega) were used for testing TCF/LEF transcriptional activity. pCAGIG-Venus was provided by Dr. Zhigang Xie (Boston University, MA). The membrane-bound GFP (pCAGIG-GAP 43-GFP) construct was gift from A. Gartner (University of Leuven, Belgium). pCAG- β -catenin (gift of Dr. Karuna Singh) was constructed by cloning β -catenin DNA sequence containing a stabilizing S37A mutation upstream of the IRES in pCAGIG.

Antibodies and Reagents

The following primary antibodies were used in this study: rabbit anti-CHD8 antibody (A301-224A, Bethyl Laboratories; ChIP), rabbit anti-Chd8 antibody (non-commercialized, Cell Signaling; 1:1000 dilution; WB), chicken anti-GFP antibody (GFP-1020, Aves Labs; 1:1000 dilution; IHC), mouse anti-BrdU antibody (M0744, Clone Bu20a, DakoCytomation; 1:500; IHC), rabbit anti-Ki67 antibody (Clone SP6, Lab Vision/Thermo Scientific; 1:500 dilution; IHC), rabbit anti-phospho-Histone H3 (Ser10) antibody (06–570, Millipore; 1:500 dilution; IHC), mouse anti-Tuj1 antibody (MMS-435P, Covance; 1:500 dilution; IHC), mouse anti-EZH2 antibody (AC22, Active Motif; 1:500 dilution, WB). Alexa-conjugated secondary antibodies (Jackson ImmunoResearch; 1:1000 dilution) were used for IHC and ICC. Recombinant mouse Wnt-3a was purchased from R&D Systems (Catalog number: 1324-WN). BrdU (5-Bromo-2'-deoxyuridine) was purchased from Sigma-Aldrich (B5002-5G).

Animals

All animal work was approved by the Committee for Animal Care of the Division of Comparative Medicine at the Massachusetts Institute of Technology. Swiss Webster pregnant female mice were purchased from Taconic (Hudson, NY, USA) for *in utero* electroporation. Mice were housed in groups of 3–4 on standard 12h light / 12 h dark cycle.

In situ hybridization probe design

RNA antisense probes were generated by PCR-amplifying mouse cDNA with primers to amplify exons 3–10 of the long isoform of *Chd8* (Supplemental Table 1). The reverse primer contains a T7 RNA polymerase recognition sequence (TAATACGACTCACTATAGGG, Supplemental Table 1). The resulting PCR product was gel extracted and *in vitro* transcribed using a DIG-RNA labeling kit (Roche).

In situ hybridization

E12 embryos and E16 brains were fixed overnight in RNase-free 4% formaldehyde. Brains were equilibrated in 30% sucrose-PBS and frozen in O.C.T. (TissueTek). Cryosections

(10 μ m) were incubated with the DIG-labeled RNA antisense probe (1:1000 in hybridization buffer) overnight at 65°C, washed in 1X SSC/50% formamide/0.1% Tween-20 3 \times 30 minutes at 65°C followed by 1X MABT for 30 minutes at room temperature. Sections were blocked with 20% heat-inactivated sheep serum/2% blocking reagent (Roche)/1X MABT for 1 hour and then incubated with anti-DIG antibody (Roche; 1:2000) overnight. Sections were washed with 1XMABT 4 \times 20 minutes, prestained with 100mM NaCl/50mM MgCl₂/100mM Tris pH 9.5/0.1% Tween-20 2 \times 10 minutes, followed by staining with NBT/BCIP (Roche; 4.5 μ l/ml and 3.5 μ l/ml, respectively, in prestaining buffer) for 2 hours. Sections were washed with 1X PBS 3 \times 15 minutes, incubated in xylene 3 \times 5 minutes, and mounted with VectaMount (Vector Laboratories).

***In utero* Electroporation**

The Institutional Animal Care and Use Committee of Massachusetts Institute of Technology approved all experiments. *In utero* electroporation was performed as described elsewhere⁵¹. Briefly, pregnant Swiss Webster mice were anesthetized by intraperitoneal injections of Ketamine 1% / Xylazine 2 mg/ml, the uterine horns were exposed, and the plasmids mixed with Fast Green (Sigma) were microinjected into a single lateral ventricle of embryos for neurogenesis and luciferase experiments. Bilateral targeting was achieved by simultaneously microinjecting into both lateral ventricles followed by delivery of current while the electrodes are placed in the middle of two hemispheres. Five pulses of current (50 ms on / 950 ms off) were delivered across the head of the embryos using 5mm diameter platinum plate electrodes (CUY650-P5, Protech International Inc). The following voltages were used for different ages: 28–30 V for E13 and 32–35 for E15. In the DNA mixture, the shRNA plasmid concentration was 2 to 3-fold higher than that of pCAGIG-Venus and membrane bound-GFP. For rescue experiments with stabilized β -catenin, the ratio between the *Chd8* shRNA and β -catenin was 5:1 in co-expression DNA mixture. For rescue experiments with h*CHD8*, the ratio between the *Chd8* shRNA and h*CHD8* was 3:1 in co-expression DNA mixture. For *in vivo* TCF/LEF luciferase assay, following ratio is used; shRNA or overexpression constructs (15) : pCAGIG-Venus (3) : 8XSuperTOPFLASH (3) : pRL-TK (1).

Cell Culture

N2A embryonic carcinoma cell line and human embryonic kidney (HEK) 293T cell line were cultured in Dulbecco's Modified Eagle Medium (DMEM) GlutaMAX (10566-016, Life Technologies) containing 10% FBS and penicillin/streptomycin. Cortical mouse NPCs were cultured using E14 mouse cortex in poly-L-ornithine coated plates and maintained in Neurobasal medium (21103-049, Life Technologies) containing 1% penicillin/streptomycin, 1% L-Glutamine, 1% N-2 supplement, 1% B27 and 10ng/ml bFGF. Human NPCs were plated at 3 \times 10⁵ per well of 24-well plate coated with matrigel. hNPCs were cultured in DMEM/F12 Glutamax (10565-042, Life technologies) containing 1% penicillin/streptomycin, 0.5% non-essential amino acid, 0.5% N2-supplement, 1% B27, 0.00025% insulin. An absence of mycoplasma in all cell lines was routinely assessed in the lab by Hoechst staining.

qRT-PCR

Total RNA was collected using the Rneasy Plus Kit (Qiagen). For knockdown experiments with shRNAs, total RNA was collected 48 hours after transfection. Reverse transcription of the mRNA transcripts to produce cDNA for QPCR was achieved using the SuperScript III Reverse Transcriptase (Invitrogen). qPCR was performed using SsoFast Evagreen Supermix (Bio-Rad) on CFX96 Real-Time PCR Detection System (Bio-Rad). The reactions were run in triplicates and average of these triplicates were used for statistical analysis. β -actin was used as internal control. Primer sequences used for qPCR can be found in Supplemental Table 1.

Immunohistochemistry

Brain Sections—Following dissection, embryonic cortical brains were drop-fixed overnight in 4% paraformaldehyde (PFA) and then transferred to 30% sucrose/PBS solution at 4°C. Brains were embedded in O.C.T. compound (Electron Microscopy Sciences) and sliced into 14 μ m sections using cryostat. Cryosections were rehydrated with 1X PBS and blocked for 1 – 2 hours with blocking solution (1X PBS + 10% Donkey Normal Serum + 0.3% Triton-X). Following blocking, the cryosections were incubated with primary antibodies overnight at 4°C. Incubation with secondary antibodies were performed for 1 hour at room temperature. Finally, cryosections were mounted using ProLong Gold Antifade Reagent (Invitrogen).

Fluorescent-activated Cell Sorting (FACS)

GFP transfected cortices from E15 embryos electroporated at E13 were micro-dissected using a fluorescent dissection microscope to increase concentration of GFP-labeled cells. Cortices from 3–5 embryos were pooled and cells were enzymatically dissociated and resuspended in HBSS. GFP-positive cells were isolated using the FACS Aria 1 (BD Biosciences) system. Gating for GFP fluorescent cells was set using non-transfected cortical cells. Cells were directly sorted into RLT (QIAGEN RNeasy Plus Kit) buffer.

Genome-Wide RNA-sequencing and Bioinformatic Analyses

Following total RNA isolation from FAC sorted GFP-positive cells using Rneasy Plus Kit (Qiagen), RNA was quality controlled and quantified using an Agilent 2100 Bioanalyzer. Next, poly-A purified samples were converted to cDNA using the Clontech Low Input Library Prep Kit (Cat#: 634947) by MIT BioMicro Center. High-throughput sequencing was performed using the Illumina HiSeq 2000 platform at the MIT BioMicro Center. The raw FASTQ data files of 40-bp or 75-bp pair-end reads were collected for downstream analysis. Sequencing reads were aligned to the mouse genome assembly (mm9) using TopHat2 (version 2.0.12⁵²) with inner distance between mate pairs=200, segment length=20, no coverage search to speed up the process, and default for other parameters. Differential expression analysis was performed using Cuffdiff module of Cufflinks (version 2.1.1⁵³) with default parameters, and FPKM values were normalized by the geometric method that Cuffdiff recommends. Significantly altered genes were the genes with both fold change greater than 1.2 and P-value less than 0.05 between two groups. See below for details:

Number of Genes for differential analysis	sh1	sh2
# of genes "NOTEST" (not enough alignments for testing, threshold 10)	10500	9377
# of genes "LOWDATA" (too complex or shallowly sequenced, default setting of cuffdiff)	0	0
# of genes "HIDATA" (too many fragments in locus, threshold 500000)	1	0
# of genes "FAIL" (ill-conditioned covariance matrix or other numerical exception prevents testing, default)	3	1
# of filtered genes "OK" for differential expression test	12731	13857
# of tested genes with at least 1.2 fold change between WT and KD groups	5615	10850
# of differentially expressed genes with at least 1.2 fold change & $p < 0.05$	3762	5245

Comparisons of each biological replicate showed Pearson coefficient of higher than 0.65 (Supplementary Figure 4b). To compare to human datasets, mouse gene names were converted to human homologs using MGI annotation database (www.informatics.jax.org/homology.shtml). Gene ontology was assessed using ToppGene and DAVID web servers. The raw data are available online (NCBI GEO GSE72442).

Human brain data link to Chd8 KD RNA-Seq data

Human developmental transcriptome dataset (Gencode v10, summarized to genes) was acquired from BRAINSPAN database (<http://www.brainspan.org/static/download.html>). *CHD8* expression patterns from early fetal stage to childhood were extracted for comparison. SFARI ASD risk gene list was acquired from SFARI gene database (<http://gene.sfari.org>). Statistical significance of overlap between human ASD risk genes and human homologs of mouse *Chd8* knockdown RNA-Seq genes was calculated using hypergeometric probability test.

Mouse E12 forebrain chromatin state analysis

Mouse E12 forebrain ChIP-Seq raw data of seven histone marks (H3K4me1, H3K4me2, H3K4me3, H3K27ac, H3K27me3, H3K9ac, and H3K36me3) were downloaded from ENCODE (www.encodeproject.org, contributed by Bing Ren group) and mapped to mouse genome assembly (mm9) using BWA aligner (version 5, samse option)⁵⁴. Duplicate reads were removed using Samtools⁵⁵. Mouse genome segmentation based on combinatorial histone marks was trained using ChromHMM³³ with the default parameters. In brief, sequencing reads were counted in non-overlapping 200-bp bins across the whole genome; each bin was binarized with either 1 for enriched or 0 for non-enriched based on a Poisson *P*-value (threshold 1×10^{-4}) that compares ChIP-Seq signals against whole-cell extract signals. Models with different numbers of states (from 10 to 14) were tested, and a model with 13 states was chosen. Annotation of those chromatin states was based on known classification of histone marks and relative enrichment of genic and non-genic regions of reference genes. Mouse *Chd8*, *Ezh2*, and *Suz12* ChIP-Seq peak files were directly downloaded or called using raw data files downloaded from GEO database (GSE57369¹², GSE31655³⁴, GSE27148³⁵, mm9 assembly) for chromatin state enrichment analysis.

Human Chd8 ChIP-Seq peak files (GSE57369¹², GSE61487 (overlap of three antibodies)¹⁶) were converted to mm9 assembly using liftover tool for enrichment analysis.

Overlap of ChIP-Seq data with Chd8 KD RNA-Seq data

ChIP-Seq peaks were further associated to the nearest annotated genes based on the distance to the transcription start sites using HOMER⁵⁶ for overlap analysis with RNA-Seq data. Histone ChIP-Seq signal intensity files (bedgraph format, normalized against input data) were generated using MACS2 program⁵⁷. A custom PERL script embedded into NeuEpi-Analyzer (<http://bioinfopilm46.mit.edu/neuepi>) was used to calculate ChIP-Seq signal intensity around transcription start sites (TSS) for all annotated genes. Intensity signals in each 100-bp bin were averaged for a detection window ranging from -5kb to 5kb around TSS. To compare ChIP-Seq signals for different gene groups, aggregated average bin signals across all the genes in a particular group were computed and plotted using a custom R script. Unless specified, overlapped genes were counted using NeuVenn-Analyzer (bioinfopilm46.mit.edu/neuvenn).

Chromatin Immunoprecipitation (ChIP)

Chromatin immunoprecipitation was performed using SimpleChIP Plus Enzymatic Chromatin IP Kit (Magnetic Beads, 9005, Cell Signaling Technology) as described by the manufacturer. Briefly, tissue from 6 mouse cortices (embryonic day 12) were pooled for each experiment. Cortical cell samples were finely minced and crosslinked with formaldehyde (1.5% final concentration) for 20 min at room temperature, chilled on ice with 10X glycine and washed once with ice cold PBS. Samples were passed through 30G needle to homogenize and create single cell suspension. Cells were resuspended in 1X Buffer A containing 0.1 mM DTT and incubated on ice for 10 min, followed by incubation in 1X Buffer B containing 0.1 mM DTT. Micrococcal Nuclease was added to mix and incubated for 20 min at 37°C vortexing every 3 min. The reaction was stopped with 50 mM EDTA (final concentration). Centrifuged pellet was resuspended in 1× ChIP buffer containing protease inhibitor cocktail. Resuspended nuclei were sonicated using a bioruptor (medium power, 30 seconds on/30 seconds off – 10 cycles). Sheared chromatin was immunoprecipitated with 5 µg antibodies against Chd8 (A301-224A, Bethyl Laboratories) and IgG overnight at 4°C. Next day, ChIP grade protein G magnetic beads were added and incubated for 2 hours at 4°C. Crosslinked protein-DNA complexes were eluted from the beads using 1X ChIP elution buffer, and incubated 65°C for 30 min, followed by reversion of crosslinking with NaCl and Proteinase K (65°C for 2 hours). Finally, DNA was purified and samples were subjected to qRT-PCR using the indicated primer (Supplementary Table 1).

Western Blot Analysis

Transfected cells were lysed and run on 6% sodium dodecylsulfate-polyacrylamide gels at 60–120 constant voltage to separate, and transferred onto Immobilon-P PVDF membranes (Millipore) at a constant voltage (80 volt for 6 hours). Membranes were blocked using 3% bovine serum albumin prepared in TBS-T (50 mM Tris-HCl (pH 7.4), 150 mM NaCl, 0.1% Tween-20) for 1 hour at room temperature. Membranes were incubated with the primary antibodies overnight at 4 °C. Next, they were washed three times with TBS-T, followed by

incubation with horseradish peroxidase-conjugated secondary antibodies (GE Healthcare, Pittsburgh, PA, USA) for 1 h at room temperature. Following washing with TBS-T, immunoreactivity signals were detected by enhanced chemiluminescence (Perkin-Elmer, Waltham, MA, USA).

Luciferase Assay

Luciferase assays were performed as described elsewhere⁵⁸.

In vitro—N2a and HEK293T cells at 1×10^5 , mNPC and hNPC at 3×10^5 cells per well density were plated into 24-well plates without antibiotics. Cells were transfected with 0.8 μ g of shRNA plasmid along with 50 ng of Super8XTOPFLASH and 10 ng of pRL-TK. The media were replaced with one containing antibiotics 2 h after transfection. 36 h after transfection, cells were stimulated with recombinant mouse Wnt3a for 12 h, in Wnt-stimulated condition. For the rescue experiments with h*CHD8*, 0.2 μ g of h*CHD8* was co-transfected with 0.6 μ g of *Chd8* shRNA. For the rescue experiments with S/A β -catenin, 0.1 μ g of S/A β -catenin was co-transfected with 0.7 μ g of *Chd8* shRNA.

In vivo—Following ratio is used; shRNA or overexpression constructs (15) : pCAGIG-Venus (3) : 8XSuperTOPFLASH (3) : pRL-TK (1). *In utero* electroporation was done at E13 and GFP-positive cortical region was dissected using fluorescent dissection microscopy to enrich for luciferase activity. Tissue was lysed using 1X Passive Lysis Buffer (E1941, Promega). TCF/LEF reporter activity was measured using the Dual-Luciferase Reporter Assay System (Promega). Firefly luciferase activity was normalized to Renilla luciferase activity in all conditions.

Behavioral Experiments

For Behavioral analysis of *Chd8* knockdown and Control mice, 10-week old animals were used. Detailed information on the ages of animals can be found on Supplemental Table 2. All animals were handled for 3 days before each experiment. All behavioral experiments were performed during the light cycle. Investigator was blinded to the group allocation during both the experiment and assessing the outcome. Ear-tag identification numbers were used until outcome analysis were finalized. Mice that were tested on multiple behavioral paradigms were given a minimum of 1 week resting period between experiments. 3 animals for control condition and 4 animals for *Chd8* shRNA condition were excluded from the study due to unsuccessful bilateral targeting of cortex (i.e. GFP+ cell only in one hemisphere or no transfection), and randomization of experimental groups was not required.

Open Field Test—Mice were placed in an open field arena (40 cm \times 40 cm \times 30 cm) and activity was measured over 10 min period with VersaMex software (AccuScan Instruments, OH). Total time moving, total distance, time spent in center and margin were measured in 5 min bins using a grid of infrared light beams and analyzed using the software.

Light-Dark Exploration Test—An apparatus (40 cm \times 40 cm) consisting of two chambers - a black box (20cm \times 20 cm) covering half of the arena and light chamber - was used for light/dark exploration test. A mouse was placed into the dark side, and allowed to

explore the arena for 10 min. The number of visits to light chamber and the time spent in the light and dark chambers were measured.

Elevated Plus Maze—Mice were allowed to explore the elevated plus maze apparatus consisting of four arms (two open and two closed arms; each arm 45 cm × 9.5 cm; the height of closed arms 29.5 cm). The activity of mice were recorded for 10 min. Time spent and number of entries to each arm was hand scored following the experiment. An entry was defined as a mouse having front paws and half of the body on the arms.

Three-chamber Social Interaction—The three-chamber social interaction apparatus consisted of black acrylic box with three chambers (20 cm × 35 cm). Side chambers were connected to middle chamber through 5 cm openings which can be closed or open. The wired cages placed in the side chambers were cylindrical with bottom diameter of 10 cm, and bars were spaced 1 cm apart. For testing, test animals were placed into the middle chamber and allowed to habituate/explore the empty arena (with empty wired cages in place) for 10 min. Following the first 10 min, an aged matched novel mouse (Stranger) was placed into one of the wired cages, and an inanimate object in the other wired cage. The test animal was allowed to explore for an additional 10 min. Activity of the mice were video recorded. Time spent in each chamber and time spent in close interaction with wired cage (within 5 cm and facing the wired cages) were hand scored using the recorded videos.

Confocal Imaging

Images were taken with a Zeiss LSM 510 confocal microscope. Brightness and contrast were adjusted using ImageJ where needed.

Statistics

All plots were generated and statistical analyses were performed using Graphpad Prism 5.0 software. Results are presented as mean ± s.e.m. Sample size was not predetermined but number of samples are consistent with previous publications. Two-tailed *t* test was used for comparison of two datasets. One-way ANOVA followed by either Dunnett (when comparing to control condition) or Bonferroni multiple comparison tests were used for experiments with three or more datasets. Equal variance between groups and normal distribution of data were presumed but not formally tested. Molecular and biochemical analysis was performed using a minimum of three biological replicates per condition. Behavioral experiments require larger data sets due to increased variability. Minimum of 6 animals per group were used for behavioral testing. Significance threshold was set to $p=0.025$ to correct for two parameters used for each behavioral test.

Supplementary Material

Refer to Web version on PubMed Central for supplementary material.

Acknowledgments

We thank Drs., R. Madabhushi, J. Penney and A. Mungenast for critical reading of the manuscript. We are thankful to R. Madabhushi, J.D. Cheng, J. Penney and Y. T. Lin for technical help and suggestions with the project. Super8xTOPFLASH luciferase reporter construct was a kind gift from Dr. Randall Moon (University of

Washington, WA). OD is a Henry Singleton (1940) Fellow (Brain and Cognitive Sciences, Massachusetts Institute of Technology). YJKW and LAW were supported by a postdoctoral fellowship from the Simons Foundation (Simons Center for the Social Brain, Massachusetts Institute of Technology). LAW is supported by postdoctoral fellowship from Natural Science and Engineering Council of Canada. We would like to thank the JPB Foundation for supporting our study. This work was partially supported by a NIH U01 grant (MH106018-03) to L.-H.T.

References

1. Miles JH. Autism spectrum disorders—a genetics review. *Genet Med.* 2011; 13:278–294. [PubMed: 21358411]
2. Watts TJ. The pathogenesis of autism. *Clin Med Pathol.* 2008; 1:99–103. [PubMed: 21876658]
3. Sanders SJ, et al. De novo mutations revealed by whole-exome sequencing are strongly associated with autism. *Nature.* 2012; 485:237–241. [PubMed: 22495306]
4. O’Roak BJ, et al. Sporadic autism exomes reveal a highly interconnected protein network of de novo mutations. *Nature.* 2012; 485:246–250. [PubMed: 22495309]
5. O’Roak BJ, et al. Multiplex targeted sequencing identifies recurrently mutated genes in autism spectrum disorders. *Science.* 2012; 338:1619–1622. [PubMed: 23160955]
6. Neale BM, et al. Patterns and rates of exonic de novo mutations in autism spectrum disorders. *Nature.* 2012; 485:242–245. [PubMed: 22495311]
7. Talkowski ME, et al. Sequencing chromosomal abnormalities reveals neurodevelopmental loci that confer risk across diagnostic boundaries. *Cell.* 2012; 149:525–537. [PubMed: 22521361]
8. De Rubeis S, et al. Synaptic, transcriptional and chromatin genes disrupted in autism. *Nature.* 2014; 515:209–215. [PubMed: 25363760]
9. Bernier R, et al. Disruptive CHD8 mutations define a subtype of autism early in development. *Cell.* 2014; 158:263–276. [PubMed: 24998929]
10. Kobayashi M, et al. Nuclear localization of Duplin, a beta-catenin-binding protein, is essential for its inhibitory activity on the Wnt signaling pathway. *J Biol Chem.* 2002; 277:5816–5822. [PubMed: 11744694]
11. Subtil-Rodríguez A, et al. The chromatin remodeller CHD8 is required for E2F-dependent transcription activation of S-phase genes. *Nucleic Acids Res.* 2014; 42:2185–2196. [PubMed: 24265227]
12. Cotney J, et al. The autism-associated chromatin modifier CHD8 regulates other autism risk genes during human neurodevelopment. *Nat Commun.* 2015; 6:6404. [PubMed: 25752243]
13. Sakamoto I, et al. A novel β -catenin-binding protein inhibits β -catenin-dependent Tcf activation and axis formation. *J Biol Chem.* 2000; 275:32871–32878. [PubMed: 10921920]
14. Nishiyama M, et al. Early embryonic death in mice lacking the β -catenin-binding protein Duplin. *Mol Cell Biol.* 2004; 24:8386–8394. [PubMed: 15367660]
15. Rodríguez-Paredes M, Ceballos-Chávez M, Esteller M, García-Domínguez M, Reyes JC. The chromatin remodeling factor CHD8 interacts with elongating RNA polymerase II and controls expression of the cyclin E2 gene. *Nucleic Acids Res.* 2009; 37:2449–2460. [PubMed: 19255092]
16. Sugathan A, et al. CHD8 regulates neurodevelopmental pathways associated with autism spectrum disorder in neural progenitors. *Proc Natl Acad Sci USA.* 2014; 111:E4468–E4477. [PubMed: 25294932]
17. Courchesne E, et al. Neuron number and size in prefrontal cortex of children with autism. *J Am Med Assoc.* 2011; 306:2001–2010.
18. Courchesne E, Carper R, Akshoomoff N. Evidence of brain overgrowth in the first year of life in autism. *J Am Med Assoc.* 2003; 290:337–344.
19. Dehay C, Kennedy H. Cell-cycle control and cortical development. *Nat Rev Neurosci.* 2007; 8:438–450. [PubMed: 17514197]
20. Kriegstein A, Noctor S, Martínez-Cerdeño V. Patterns of neural stem and progenitor cell division may underlie evolutionary cortical expansion. *Nat Rev Neurosci.* 2006; 7:883–890. [PubMed: 17033683]
21. Hardwick LJA, Philpott A. Nervous decision-making: to divide or differentiate. *Trends Genet.* 2014; 30:254–261. [PubMed: 24791612]

22. Niehrs C, Acebron SP. Mitotic and mitogenic Wnt signalling. *EMBO J.* 2012; 31:2705–2713. [PubMed: 22617425]
23. Chenn A. Wnt/ β -catenin signaling in cerebral cortical development. *Organogenesis.* 2008; 4:76–80. [PubMed: 19279718]
24. Munji RN, Choe Y, Li G, Siegenthaler JA, Pleasure SJ. Wnt signaling regulates neuronal differentiation of cortical intermediate progenitors. *J Neurosci.* 2011; 31:1676–1687. [PubMed: 21289176]
25. Hirabayashi Y, et al. The Wnt/ β -catenin pathway directs neuronal differentiation of cortical neural precursor cells. *Development.* 2004; 131:2791–2801. [PubMed: 15142975]
26. Chenn A, Walsh CA. Regulation of cerebral cortical size by control of cell cycle exit in neural precursors. *Science.* 2002; 297:365–369. [PubMed: 12130776]
27. Hirabayashi Y, Gotoh Y. Epigenetic control of neural precursor cell fate during development. *Nat Rev Neurosci.* 2010; 11:377–388. [PubMed: 20485363]
28. Pereira JD, et al. Ezh2, the histone methyltransferase of PRC2, regulates the balance between self-renewal and differentiation in the cerebral cortex. *Proc Natl Acad Sci USA.* 2010; 107:15957–15962. [PubMed: 20798045]
29. Kang HJ, et al. Spatio-temporal transcriptome of the human brain. *Nature.* 2011; 478:483–489. [PubMed: 22031440]
30. Wang P, et al. CRISPR/Cas9-mediated heterozygous knockout of the autism gene CHD8 and characterization of its transcriptional networks in neurodevelopment. *Mol Autism.* 2015; 6:55. [PubMed: 26491539]
31. Wilkinson B, et al. The autism-associated gene chromodomain helicase DNA-binding protein 8 (CHD8) regulates noncoding RNAs and autism-related genes. *Transl Psychiatry.* 2015; 5:e568. [PubMed: 25989142]
32. Abrahams BS, et al. SFARI Gene 2.0: a community-driven knowledgebase for the autism spectrum disorders (ASDs). *Mol Autism.* 2013; 4:36. [PubMed: 24090431]
33. Ernst J, Kellis M. ChromHMM: automating chromatin-state discovery and characterization. *Nat Methods.* 2012; 9:215–216. [PubMed: 22373907]
34. Sher F, Boddeke E, Olah M, Copray S. Dynamic changes in Ezh2 gene occupancy underlie its involvement in neural stem cell self-renewal and differentiation towards oligodendrocytes. *PLoS One.* 2012; 7:e40399. [PubMed: 22808153]
35. Arnold P, et al. Modeling of epigenome dynamics identifies transcription factors that mediate Polycomb targeting. *Genome Res.* 2013; 23:60–73. [PubMed: 22964890]
36. Thompson BA, Tremblay V, Lin G, Bochar DA. CHD8 is an ATP-dependent chromatin remodeling factor that regulates β -catenin target genes. *Mol Cell Biol.* 2008; 28:3894–3904. [PubMed: 18378692]
37. Nishiyama M, Skoultchi AI, Nakayama KI. Histone H1 recruitment by CHD8 is essential for suppression of the Wnt- β -catenin signaling pathway. *Mol Cell Biol.* 2012; 32:501–512. [PubMed: 22083958]
38. Bourin M, Hascoët M. The mouse light/dark box test. *Eur J Pharmacol.* 2003; 463:55–65. [PubMed: 12600702]
39. Walf AA, Frye CA. The use of the elevated plus maze as an assay of anxiety-related behavior in rodents. *Nat Protoc.* 2007; 2:322–328. [PubMed: 17406592]
40. Moy SS, et al. Sociability and preference for social novelty in five inbred strains: an approach to assess autistic-like behavior in mice. *Genes Brain Behav.* 2004; 3:287–302. [PubMed: 15344922]
41. Yu X, Malenka RC. Beta-catenin is critical for dendritic morphogenesis. *Nat Neurosci.* 2003; 6:1169–1177. [PubMed: 14528308]
42. Rosso SB, Inestrosa NC. WNT signaling in neuronal maturation and synaptogenesis. *Front Cell Neurosci.* 2013; 7:103. [PubMed: 23847469]
43. Menon T, Yates JA, Bochar DA. Regulation of androgen-responsive transcription by the chromatin remodeling factor CHD8. *Mol Endocrinol.* 2010; 24:1165–1174. [PubMed: 20308527]

44. Fang M, Ou J, Hutchinson L, Green MR. The BRAF oncoprotein functions through the transcriptional repressor MAFG to mediate the CpG island methylator phenotype. *Mol Cell*. 2014; 55:904–915. [PubMed: 25219500]
45. Hurd EA, Poucher HK, Cheng K, Raphael Y, Martin DM. The ATP-dependent chromatin remodeling enzyme CHD7 regulates pro-neural gene expression and neurogenesis in the inner ear. *Development*. 2010; 137:3139–3150. [PubMed: 20736290]
46. Layman WS, et al. Defects in neural stem cell proliferation and olfaction in Chd7 deficient mice indicate a mechanism for hyposmia in human CHARGE syndrome. *Hum Mol Genet*. 2009; 18:1909–1923. [PubMed: 19279158]
47. Balow SA, et al. Knockdown of fbx110/kdm2bb rescues chd7 morphant phenotype in a zebrafish model of CHARGE syndrome. *Dev Biol*. 2013; 382:57–69. [PubMed: 23920116]
48. Platt JL, Rogers BJ, Rogers KC, Harwood AJ, Kimmel AR. Different CHD chromatin remodelers are required for expression of distinct gene sets and specific stages during development of *Dictyostelium discoideum*. *Development*. 2013; 140:4926–4936. [PubMed: 24301467]
49. Kalkman HO. A review of the evidence for the canonical Wnt pathway in autism spectrum disorders. *Mol Autism*. 2012; 3:10. [PubMed: 23083465]
50. Terriente-Félix A, Molnar C, Gómez-Skarmeta JL, de Celis JF. A conserved function of the chromatin ATPase Kismet in the regulation of hedgehog expression. *Dev Biol*. 2011; 350:382–392. [PubMed: 21146514]
51. Xie Z, et al. Cep120 and TACCs control interkinetic nuclear migration and the neural progenitor pool. *Neuron*. 2007; 56:79–93. [PubMed: 17920017]
52. Trapnell C, Pachter L, Salzberg SL. TopHat: discovering splice junctions with RNA-seq. *Bioinformatics*. 2009; 25:1105–1111. [PubMed: 19289445]
53. Trapnell C, et al. Differential gene and transcript expression analysis of RNA-seq experiments with TopHat and Cufflinks. *Nat Protoc*. 2012; 7:562–578. [PubMed: 22383036]
54. Li H, Durbin R. Fast and accurate short read alignment with Burrows-Wheeler transform. *Bioinformatics*. 2009; 25:1754–1760. [PubMed: 19451168]
55. Li H, et al. The sequence alignment/map format and SAMtools. *Bioinformatics*. 2009; 25:2078–2079. [PubMed: 19505943]
56. Heinz S, et al. Simple combinations of lineage-determining transcription factors prime cis-regulatory elements required for macrophage and B cell identities. *Mol Cell*. 2010; 38:576–589. [PubMed: 20513432]
57. Liu T. Use model-based Analysis of ChIP-Seq (MACS) to analyze short reads generated by sequencing protein-DNA interactions in embryonic stem cells. *Methods Mol Biol*. 2014; 1150:81–95. [PubMed: 24743991]
58. Mao Y, et al. Disrupted in schizophrenia 1 regulates neuronal progenitor proliferation via modulation of GSK3 β /catenin signaling. *Cell*. 2009; 136:1017–1031. [PubMed: 19303846]

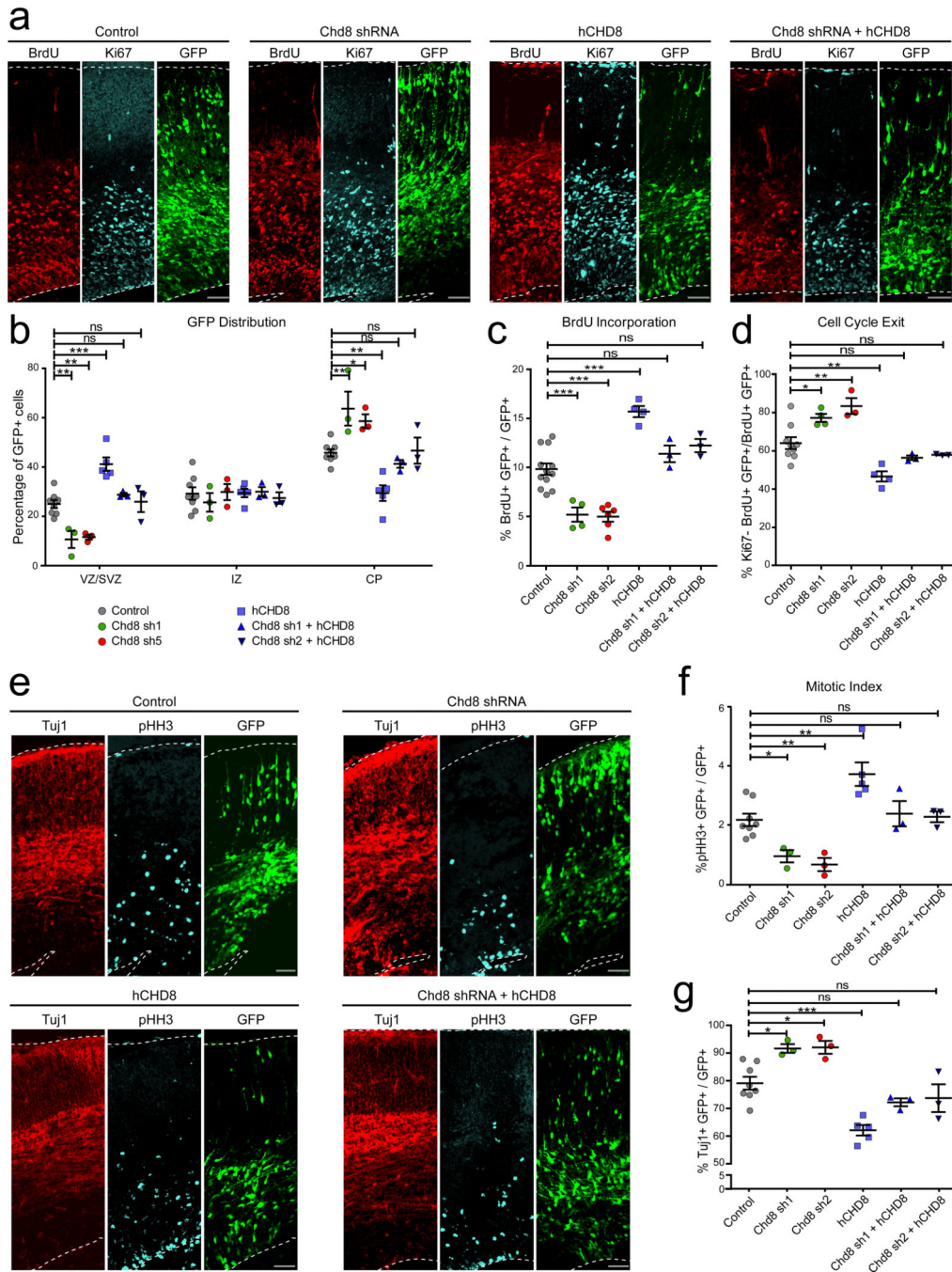


Figure 1. Chd8 regulates neural progenitor proliferation in developing cortex

(a) Images of E16 mouse cortices electroporated at E13 with nontargeting (Control), Chd8-directed small hairpin RNA (Chd8 shRNA), full-length human CHD8 construct (hCHD8), combination of Chd8 shRNA with hCHD8 (Chd8 shRNA + hCHD8) and GFP expression plasmid. Single-pulse BrdU was injected 24 h before brain dissection. Images were stained for GFP (green), BrdU (red) and Ki67 (cyan). Dashed lines represent the ventricular (bottom) and basal (top) surfaces. Scale bars: 50 μ m. (b) Distribution of GFP⁺ cell in different cortical zones 72 h after transfection at E16 shows reduced percentage of cell in

VZ/SVZ with similar increase in cortical plate (CP) following Chd8 knockdown (one-way ANOVA followed by Dunnett's multiple comparison test; DF = 5, F = 19.45, $P < 0.0001$ for VZ/SVZ; DF = 5, F = 0.2843, $P < 0.9159$ for IZ; DF = 5, F = 13.00, $P < 0.0001$ for CP; Control, n = 8; Chd8 sh1, n = 3; Chd8 sh2, n = 3; hCHD8, n = 5; Chd8 sh1 + hCHD8, n = 3; Chd8 sh2 + hCHD8, n = 3). **(c)** Chd8 knockdown resulted in decreased BrdU incorporation, which could be rescued by overexpression of hCHD8 (one-way ANOVA followed by Dunnett's multiple comparison test; DF = 5, F = 28.62, $P < 0.0001$; Control, n = 12; Chd8 sh1, n = 4; Chd8 sh2, n = 6; hCHD8, n = 4; Chd8 sh1 + hCHD8, n = 3; Chd8 sh2 + hCHD8, n = 3). **(d)** Chd8 knockdown resulted in increased cell cycle exit, which could be rescued by overexpression of hCHD8 (one-way ANOVA followed by Dunnett's multiple comparison test; DF = 5, F = 14.12, $P < 0.0001$; Control, n = 9; Chd8 sh1, n = 4; Chd8 sh2, n = 3; hCHD8, n = 4; Chd8 sh1 + hCHD8, n = 3; Chd8 sh2 + hCHD8, n = 3). **(e)** Images of E16 mouse cortices electroporated at E13. Images were stained for GFP (green), Tuj1 (red) and pHH3 (cyan). Arrows indicate GFP-pHH3 double-positive cells. Dashed lines represent the ventricular (bottom) and basal (top) surfaces. Scale bars: 50 μm . **(f)** Chd8 knockdown reduced mitotic index measured by pHH3 staining (one-way ANOVA followed by Dunnett's multiple comparison test; DF = 5, F = 11.95, $P < 0.0001$; Control, n = 8; Chd8 sh1, n = 3; Chd8 sh2, n = 3; hCHD8, n = 5; Chd8 sh1 + hCHD8, n = 3; Chd8 sh2 + hCHD8, n = 3). **(g)** Fraction of GFP⁺ cell overlapping with Tuj1 staining is increased after Chd8 knockdown (one-way ANOVA followed by Dunnett's multiple comparison test; DF = 5, F = 16.74, $P < 0.0001$; Control, n = 8; Chd8 sh1, n = 3; Chd8 sh2, n = 3; hCHD8, n = 5; Chd8 sh1 + hCHD8, n = 3; Chd8 sh2 + hCHD8, n = 3). * $P < 0.05$; ** $P < 0.01$; *** $P < 0.001$; ns., nonsignificant. n, number of different brain samples analyzed. Results are presented as mean \pm s.e.m.

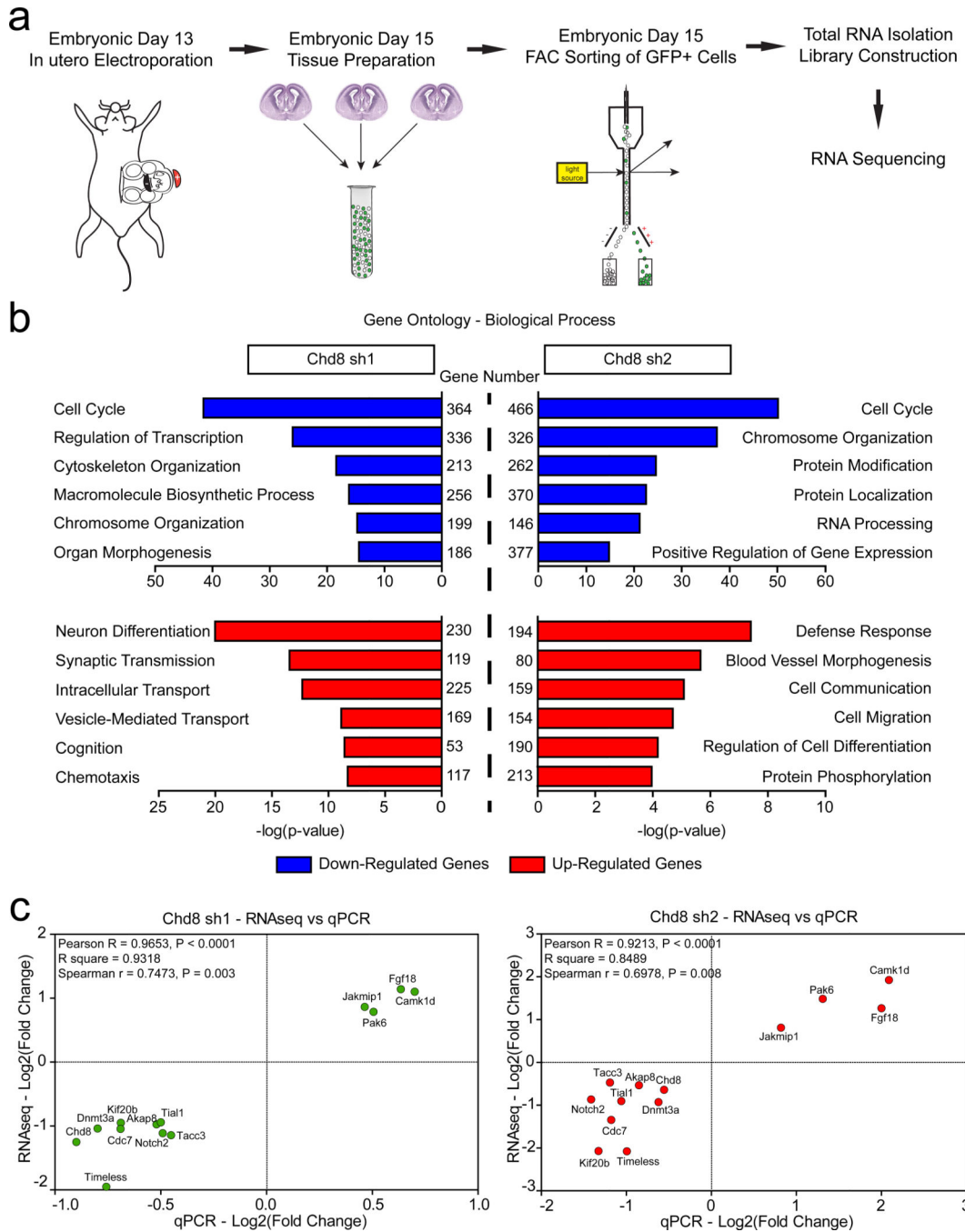


Figure 2. Chd8 is important for the expression of cell cycle genes in developing brain
(a) Schematic explaining the steps of RNA-seq experiment. **(b)** Analysis of gene ontology of biological functions for downregulated (top panel) and upregulated (bottom panel) genes from Chd8-knockdown RNA-seq data sets. **(c)** Confirmation of subset of differentially expressed genes identified by RNA-seq in independent set of samples using qRT-PCR correlated with fold change from RNA-seq data. $\log_2(\text{fold change})$ is used to create 2D plots (Chd8 sh1: Pearson $R = 0.9653$, $P < 0.0001$, $R^2 = 0.9318$, Spearman $r = 0.7473$, $P = 0.003$; Chd8 sh2: Pearson $R = 0.9201$, $P < 0.0001$, $R^2 = 0.8466$, Spearman $r = 0.6978$, $P = 0.008$).

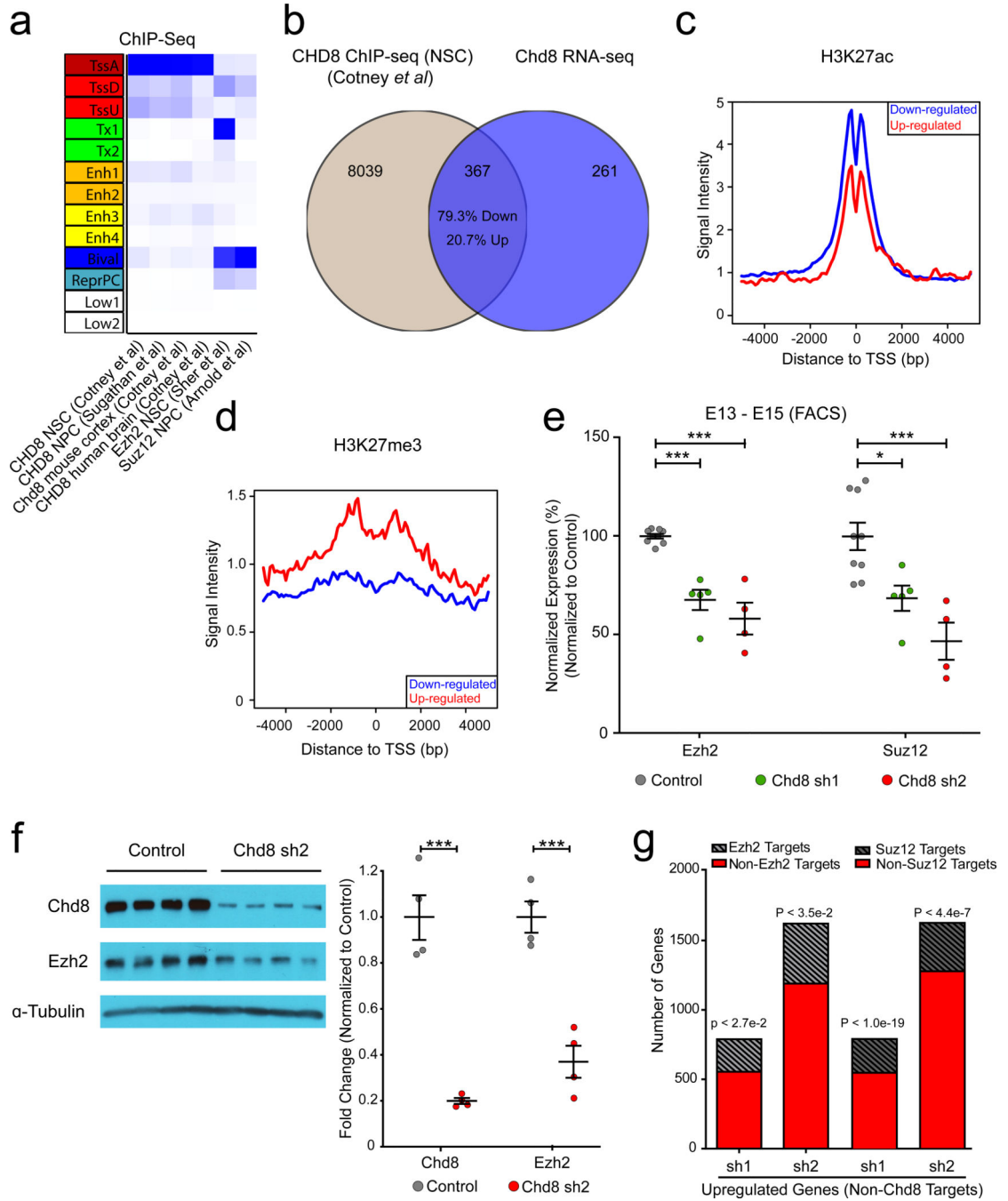


Figure 3. Direct and indirect regulation of genes necessary for early cortical development by Chd8

(a) Chromatin state enrichment analysis using CHD8 (hNSC, hNPC and midfetal human brain), Chd8 (E17.5 mouse brain), Ezh2 (hNSC) and Suz12 (hNPC) ChIP-seq peaks using published data^{12,16,34,35}. (b) Venn diagram showing the overlap between Chd8 target genes (CHD8 ChIP-seq)¹² with differentially expressed genes following Chd8-knockdown (Chd8 RNA-seq). Overlap shows enrichment of genes downregulated following Chd8 knockdown (79.5% downregulated vs. 20.5% upregulated). (c) Aggregate plots of average H3K27ac

ChIP-seq intensity signal in E12 mouse brain generated using differentially expressed genes in Chd8 RNA-seq data sets. Aggregate plots were generated at the TSS of genes upregulated (red) and downregulated (blue). TSS, transcriptional start site. **(d)** Aggregate plots of average H3K27me3 ChIP-seq intensity signal in E12 mouse brain generated using differentially expressed genes in Chd8 RNA-seq data sets. Aggregate plots were generated at the TSS of genes upregulated (red) and downregulated (blue). **(e)** Confirmation of reduced expression of Ezh2 and Suz12 in independent set of FAC-sorted Chd8-knockdown samples from embryonic brain assessed using qRT-PCR (one-way ANOVA followed by Dunnett's multiple comparison test; DF = 2, F = 32.93, P < 0.0001 for Ezh2; DF = 2, F = 12.03, P = 0.0008 for Suz12; Control, n = 9; Chd8 sh1, n = 5; Chd8 sh2, n, number of different FAC-sorted samples analyzed. **(f)** Sample western blots shown for Chd8, Ezh2 and α -tubulin (loading control, left panel). Quantification of protein expression levels normalized to α -tubulin (right panel). Knockdown of Chd8 in mouse NPCs results in reduced expression of Ezh2, a major component of polycomb repressive complex 2 (n = 4 for all samples; two-tailed student's t-test; P = 0.0002 for Chd8; P = 0.0006 for Ezh2). n, number of cultured cell samples analyzed. Full-length western blots are presented in Supplementary Figure 14. **(g)** Overlap between upregulated genes following Chd8 knockdown that are not Chd8 targets and Ezh2 or Suz12 targets^{34,35}. Ezh2 targets, 3,390 genes; Suz12 targets, 2,290 genes; upregulated genes (non-Chd8 targets) in sh1 data set, 789 genes; upregulated genes (non-Chd8 targets) in sh2 data set, 1,622 genes. P-values calculated using hypergeometric distribution test. *P < 0.05; **P < 0.01; ***P < 0.001. Results are presented as mean \pm s.e.m.

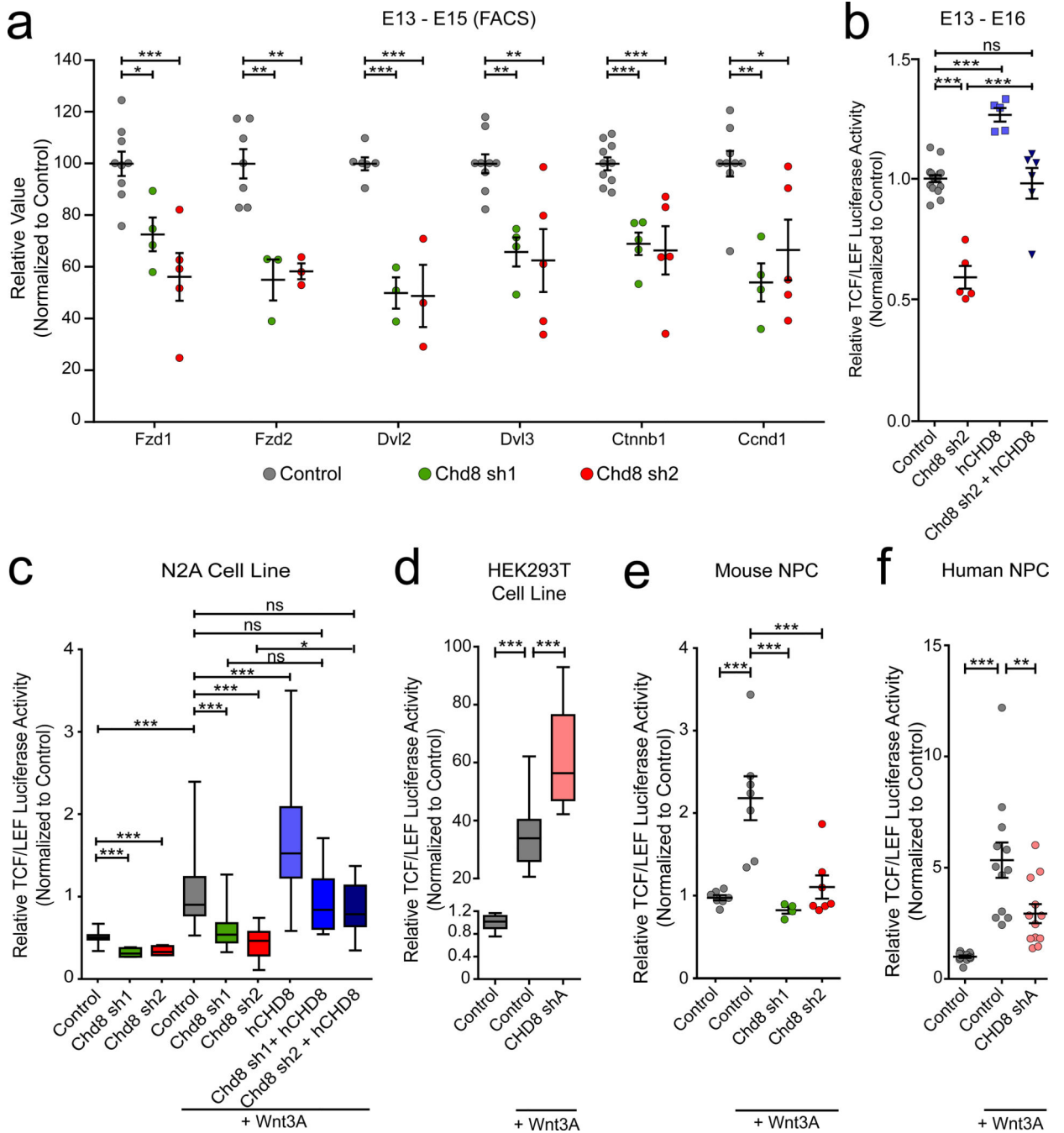


Figure 4. Chd8 is a positive regulator of canonical Wnt signaling in neuronal cells

(a) Confirmation of reduced expression of Wnt signaling genes bound by Chd8 (Fzd1, Fzd2, Dvl2, Dvl3, Ctnnb1) and a Wnt response gene (Ccnd1) in independent set of FAC-sorted Chd8-knockdown samples from embryonic brain assessed using qRT-PCR (one-way ANOVA followed by Dunnett’s multiple comparison test; DF = 2, F = 12.94, P = 0.0005 for Fzd1; DF = 2, F = 16.97, P = 0.0006 for Fzd2; DF = 2, F = 27.08, P = 0.0002 for Dvl2; DF = 2, F = 10.21, P = 0.0016 for Dvl3; DF = 2, F = 16.39, P = 0.0001 for Ctnnb1; DF = 2, F = 10.38, P = 0.0015 for Ccnd1; Control, n = 9; Chd8 sh1, n = 4; Chd8 sh2, n = 5 for Fzd1,

Dvl3 and Cend1; Control, n = 7; Chd8 sh1, n = 3; Chd8 sh2, n = 3 for Fzd2 and Dvl2; Control, n = 10; Chd8 sh1, n = 5; Chd8 sh2, n = 5 for Ctnnb1. n, number of different FAC-sorted samples analyzed. **(b)** In utero TCF/LEF luciferase assay showing that Chd8 is a positive regulator of canonical Wnt signaling (one-way ANOVA followed by Bonferroni's multiple comparison test; DF = 3, F = 47.29, P < 0.0001; Control; n = 17, Chd8 sh2; n = 5, hCHD8; n = 5, Chd8 sh2 + hCHD8; n = 6; n, number of different brain samples analyzed). **(c)** TCF/LEF luciferase assay in N2a cell line using both Chd8 shRNAs and rescue with human CHD8. Both Chd8 shRNAs resulted in reduction of Wnt activity in N2a cell line, which could be rescued via overexpression of human CHD8 (one-way ANOVA followed by Bonferroni's multiple comparison test; DF = 6, F = 53.25, P < 0.0001 for +Wnt3A; DF = 2, F = 46.64, P < 0.0001 for -Wnt3A; Control; n = 65, Chd8 sh1; n = 4, Chd8 sh2; n = 4, Control + Wnt; n = 65, Chd8 sh1 + Wnt; n = 26, Chd8 sh2 + Wnt; n = 30, hCHD8 + Wnt; n = 39, Chd8 sh1 + hCHD8 + Wnt; n = 14, Chd8 sh2 + hCHD8 + Wnt; n = 14; statistical analysis was run separately when comparing Control condition with Wnt3a- and Wnt3a+ conditions). n, number of different cultured cell samples analyzed. **(d)** TCF/LEF luciferase assay in HEK293T cell line shows increased Wnt signaling activity following CHD8 knockdown (one-way ANOVA followed by Bonferroni's multiple comparison test; DF = 2, F = 96.27, P < 0.0001; Control; n = 14, Control + Wnt; n = 14, CHD8 shA + Wnt; n = 14). n, number of different cultured cell samples analyzed. **(e)** TCF/LEF luciferase assay using cultured embryonic mouse neural progenitors showing decreased activity following Chd8 knockdown (one-way ANOVA followed by Bonferroni's multiple comparison test; DF = 3, F = 13.19, P < 0.0001; Control; n = 7, Control + Wnt; n = 7, Chd8 sh1 + Wnt; n = 4, Chd8 sh2 + Wnt; n = 7). n, number of different cultured cell samples analyzed. **(f)** TCF/LEF luciferase assay using cultured human neural progenitors showing decreased activity following Chd8 knockdown (one-way ANOVA followed by Bonferroni's multiple comparison test; DF = 2, F = 17.32, P < 0.0001; n = 12 for all conditions). n, number of different cultured cell samples analyzed. *P < 0.05; **P < 0.01; ***P < 0.001; ns., nonsignificant. Results are presented as mean ± s.e.m. (a,b,e and f). Shown are median, 25th and 75th percentile, and min and max value (c,d).

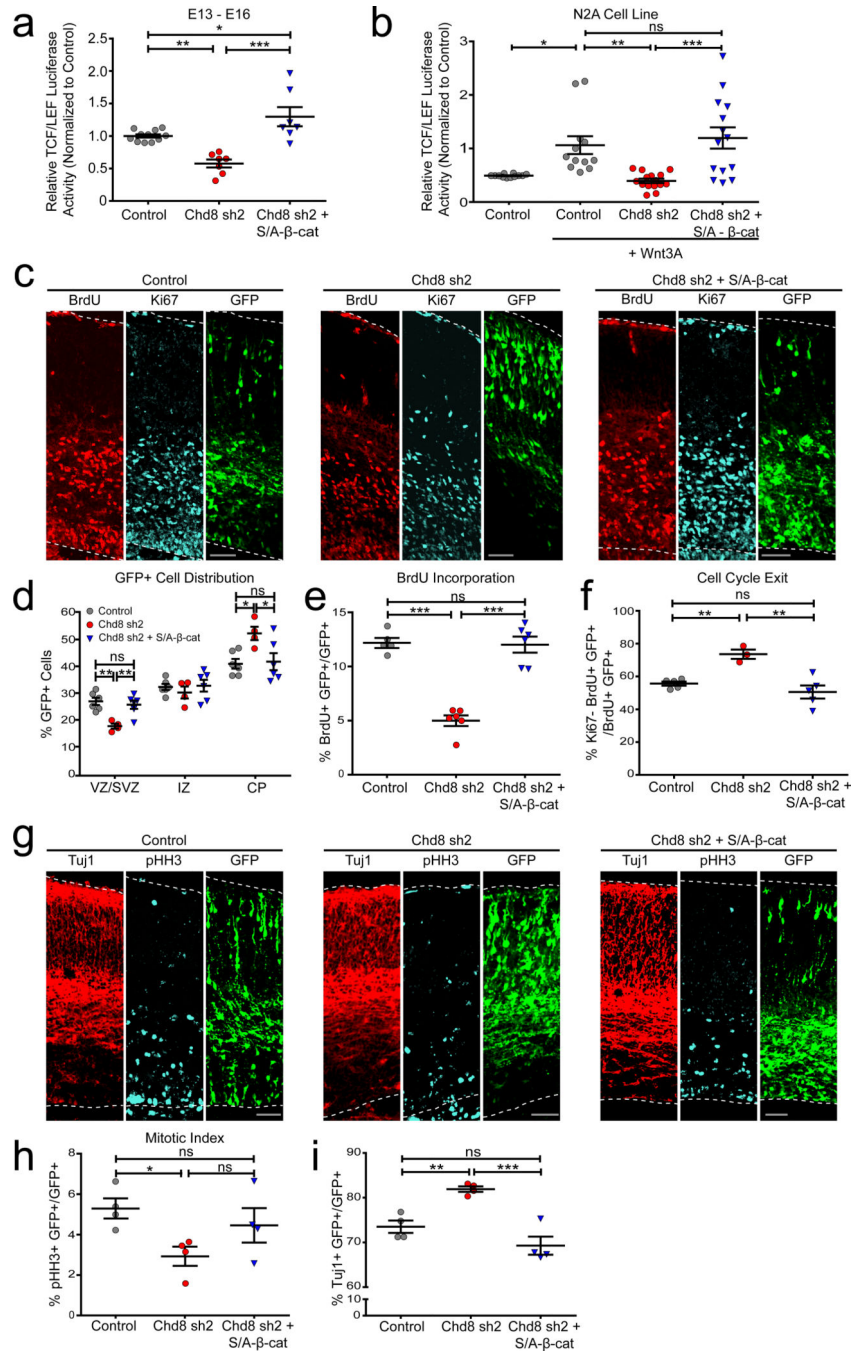


Figure 5. Increased β -catenin rescues phenotypes associated with Chd8 knockdown

(a) Stabilized β -catenin overexpression rescued reduced Wnt-mediated luciferase activity in utero (one-way ANOVA followed by Bonferroni's multiple comparison test; DF = 2, F = 17.65, P < 0.0001; Control; n = 11, Chd8 sh2; n = 7, Chd8 sh2 + β -catenin; n = 7). n, number of different cultured cell samples analyzed. (b) Stabilized β -catenin overexpression rescued reduced Wnt-mediated luciferase activity in N2a cell line (one-way ANOVA followed by Bonferroni's multiple comparison test; DF = 3, F = 9.599, P < 0.0001; Control; n = 12, Control + Wnt; n = 12, Chd8 sh2 + Wnt; n = 15, Chd8 sh2 + β -catenin; n = 14). n,

number of different cultured cell samples analyzed. **(c)** Images of E16 mouse cortices electroporated at E13 with nontargeting (Control), Chd8-directed small hairpin (Chd8 shRNA) and combination of Chd8 shRNA with stabilized β -catenin (Chd8 sh2 + S/A- β -cat) and GFP expression plasmid. Images were stained for GFP (green), BrdU (red) and Ki67 (cyan). Scale bars: 50 μ m. **(d)** Distribution of GFP⁺ cells in different cortical zones 72 h after transfection. Co-expression of stabilized β -catenin with Chd8 shRNA resulted in distribution of GFP⁺ cells indistinguishable from control condition (one-way ANOVA followed by Bonferroni's multiple comparison test; DF = 2, F = 9.772, P = 0.0026 for VZ/SVZ; DF = 2, F = 0.4438, P < 0.6410 for IZ; DF = 2, F = 4.948, P = 0.0209 for CP; Control; n = 6, Chd8 sh2; n = 4, Chd8 sh2 + β -catenin; n = 6). n, number of different brain samples analyzed. **(e)** Decreased BrdU incorporation associated with Chd8 knockdown is increased to control levels when Chd8 shRNA is co-expressed with stabilized β -catenin (one-way ANOVA followed by Bonferroni's multiple comparison test; DF = 2, F = 49.87, P < 0.0001; Control; n = 5, Chd8 sh2; n = 6, Chd8 sh2 + β -catenin; n = 6). n, number of different brain samples analyzed. **(f)** Co-expression of stabilized β -catenin with Chd8 shRNA rescues the cell cycle exit phenotype assayed using Ki67 proliferative marker (one-way ANOVA followed by Bonferroni's multiple comparison test; DF = 2, F = 13.03, P < 0.0001; Control; n = 5, Chd8 sh2; n = 3, Chd8 sh2 + β -catenin; n = 5). n, number of different brain samples analyzed. **(g)** Images of E16 mouse cortices electroporated at E13. Images were stained for GFP (green), Tuj1 (red) and pHH3 (cyan). Scale bars: 50 μ m. **(h)** Reduced mitotic index associated with Chd8 knockdown is rescued by overexpression of stabilized β -catenin (one-way ANOVA followed by Bonferroni's multiple comparison test; DF = 2, F = 4.763, P < 0.0001; Control; n = 4, Chd8 sh2; n = 4, Chd8 sh2 + β -catenin; n = 4). n, number of different brain samples analyzed. **(i)** Fraction of GFP⁺ cells overlapping with Tuj1 staining is rescued via co-expression of Chd8 shRNA with stabilized β -catenin (one-way ANOVA followed by Bonferroni's multiple comparison test; DF = 2, F = 19.43, P < 0.0001; Control; n = 4, Chd8 sh2; n = 4, Chd8 sh2 + β -catenin; n = 4). n, number of different brain samples analyzed. *P < 0.05; **P < 0.01; ***P < 0.001; ns., nonsignificant. Results are presented as mean \pm s.e.m.

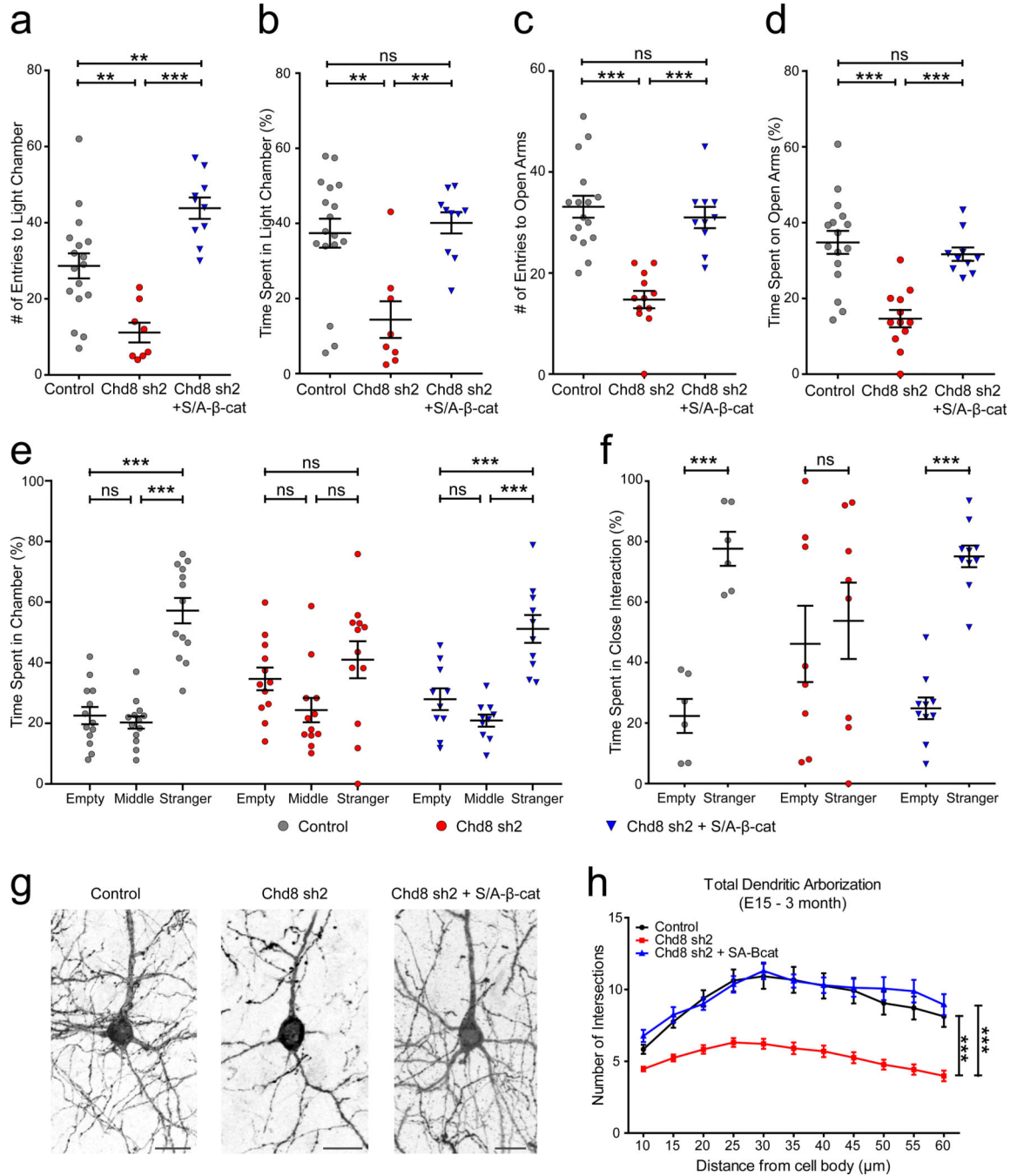


Figure 6. Chd8 Knockdown in upper cortical layer neurons results in behavioral deficits, which can be rescued via induction of Wnt signaling

(a) Chd8- knockdown mice show reduced number of entries to the light chamber in light–dark chamber assay (one-way ANOVA followed by Bonferroni’s multiple comparison test; DF = 2, F = 18.70, P < 0.0001; Control; n = 17, Chd8 sh2; n = 8, Chd8 sh2 + S/A-β-cat; n = 10). n, number of animals used. (b) Chd8-knockdown mice spent less time in the light chamber (one-way ANOVA followed by Bonferroni’s multiple comparison test; DF = 2, F = 9.521, P = 0.0006; Control; n = 17, Chd8 sh2; n = 8, Chd8 sh2 + S/A-β-cat; n = 10). n,

number of animals used. **(c)** Number of entries to the open arms in elevated plus maze assay was significantly reduced in Chd8-knockdown mice (one-way ANOVA followed by Bonferroni's multiple comparison test; $DF = 2$, $F = 23.27$, $P < 0.0001$; Control; $n = 16$, Chd8 sh2; $n = 12$, Chd8 sh2 + S/A- β -cat; $n = 10$). n , number of animals used. **(d)** Chd8 knockdown mice spent significantly less time in the light chamber (one-way ANOVA followed by Bonferroni's multiple comparison test; $DF = 2$, $F = 16.54$, $P < 0.0001$; Control; $n = 16$, Chd8 sh2; $n = 12$, Chd8 sh2 + S/A- β -cat; $n = 10$). n , number of animals used. **(e)** In the 3-chamber social interaction assay, Chd8- knockdown animals did not spend significantly more time in the chamber with the novel social animal (Stranger) relative to the chamber with the empty wire cage (Empty) compared to control or to the Chd8 sh2 + S/A- β -cat group (One-way ANOVA followed by Bonferroni's multiple comparison test; $DF = 2$, $F = 43.09$, $P < 0.0001$ for Control; $DF = 2$, $F = 3.167$, $P = 0.0552$ for Chd8 sh2; $DF = 2$, $F = 19.81$, $P < 0.0001$ for Chd8 sh2 + S/A- β -cat; Control; $n = 13$, Chd8 sh2; $n = 12$, Chd8 sh2 + S/A- β -cat; $n = 10$). n , number of animals used. **(f)** Social interaction in close proximity (within 5 cm of the wire cages). Chd8-knockdown animals did not show preference for either the Stranger or the Empty cage (Two-tailed unpaired student's t-test; $t = 6.942$, $DF = 10$, $P < 0.0001$, $n = 6$ for Control; $t = 0.4274$, $DF = 14$, $P = 0.6756$ $n = 8$ for Chd8 sh2; $t = 9.930$, $DF = 18$, $P < 0.0001$, $n = 10$ for Chd8 sh2 + S/A- β -cat). **(g)** Images of upper cortical neurons from 5-month-old mouse brains transfected at E15 with either control shRNA or Chd8 shRNA and membrane-bound GFP. Scale bars: 20 μ m. **(h)** Chd8 knockdown reduced the complexity of dendritic arborization assessed via Sholl analysis (two-way ANOVA followed by Bonferroni's multiple comparison test; $DF = 2$, sum-of-squares = 4,226, mean square = 2,113, $F = 269.5$, $P < 0.0001$ for genotype factor; Control; $n = 24$ cells from 5 animals, Chd8 sh2; $n = 52$ cells from 7 animals, Chd8 sh2 + S/A- β -cat; $n = 17$ cells from 5 animals). * $P < 0.05$; ** $P < 0.01$; *** $P < 0.001$; n.s., nonsignificant. Results are presented as mean \pm s.e.m.